Heliyon 10 (2024) e38220

Contents lists available at ScienceDirect

Heliyon

journal homepage: www.cell.com/heliyon

Research article

Novel mechanisms of intestinal flora regulation in high-altitude hypoxia

Fang Yan [a,b,1], Wen-qiang Yuan [a,b,1], Shi-min Wu [a,c], Yun-han Yang [a,b], De-jun Cui [a,b,*]

[a] Department of Gastroenterology, National Institution of Drug Clinical Trial, Guizhou Provincial People's Hospital, No.83, East Zhongshan Road, Guiyang, Guizhou, China
[b] Medical College of Guizhou University, Guiyang, Guizhou, China
[c] Zunyi Medical University, Zunyi, 563006, China

ARTICLE INFO

Keywords:
High-altitude hypoxia
Firmicutes
Mψ polarization
Glycolysis
HIF-1α

ABSTRACT

Background: This study investigates the molecular mechanisms behind firmicutes-mediated macrophage (Mψ) polarization and glycolytic metabolic reprogramming through HIF-1α in response to intrinsic mucosal barrier injury induced by high-altitude hypoxia.
Methods: Establishing a hypoxia mouse model of high altitude, we utilized single-cell transcriptome sequencing to identify key cell types involved in regulating intestinal mucosal barrier damage caused by high-altitude hypoxia. Through proteomic analysis of colonic tissue Mψ and metabolomic analysis of Mψ metabolites, we determined crucial proteins and metabolic pathways influencing intestinal mucosal barrier damage induced by high-altitude hypoxia. Mechanistic validation was conducted using RAW264.7 Mψ in vitro by assessing cell viability with CCK-8 assay following treatment with different metabolites. The hypoxia mouse model was further validated in vivo by transplanting gut microbiota of Firmicutes. Histological examinations through H&E staining assessed colonic cell morphology and structure, while the FITC-dextran assay evaluated intestinal tissue permeability. Hypoxia probe signal intensity in mouse colonic tissue was assessed via metronidazole staining. Various experimental techniques, including flow cytometry, immunofluorescence, ELISA, Western blot, and RT-qPCR, were employed to study the impact of HIF-1α/glycolysis pathway and different gut microbiota metabolites on Mψ polarization.
Results: Bioinformatics analysis revealed that single-cell transcriptomics identified Mψ as a key cell type, with their polarization pattern playing a crucial role in the intestinal mucosal barrier damage induced by high-altitude hypoxia. Proteomics combined with metabolomics analysis indicated that HIF-1α and the glycolytic pathway are pivotal proteins and signaling pathways in the intestinal mucosal barrier damage caused by high-altitude hypoxia. In vitro cell experiments demonstrated that activation of the glycolytic pathway by HIF-1α led to a significant upregulation of mRNA levels of IL-1β, IL-6, and TNFα while downregulating mRNA levels of IL-10 and TGFβ, thereby promoting M1 Mψ activation and inhibiting M2 Mψ polarization. Further mechanistic validation experiments revealed that the metabolite butyric acid from Firmicutes bacteria significantly downregulated the protein expression of HIF-1α, GCK, PFK, PKM, and LDH, thus

* Corresponding author. Department of Gastroenterology, Guizhou Provincial People's Hospital, No.83, East Zhongshan Road, Nanming District, Guiyang, 550002, Guizhou Province, China.
E-mail address: hxcuidj@163.com (D.-j. Cui).
[1] These authors are regarded as co-first authors.

https://doi.org/10.1016/j.heliyon.2024.e38220
Received 5 March 2024; Received in revised form 18 September 2024; Accepted 19 September 2024
Available online 20 September 2024

inhibiting the HIF-1α/glycolytic pathway that suppresses M1 Mψ and activates M2 Mψ, consequently alleviating the hypoxic symptoms in RAW264.7 cells. Subsequent animal experiments confirmed that Firmicutes bacteria inhibited the HIF-1α/glycolytic pathway to modulate Mψ polarization, thereby mitigating intestinal mucosal barrier damage in high-altitude hypoxic mice. *Conclusion:* The study reveals that firmicutes, through the inhibition of the HIF-1α/glycolysis pathway, mitigate Mψ polarization, thereby alleviating intrinsic mucosal barrier injury in high-altitude hypoxia.

1. Introduction

High-altitude hypoxia refers to the condition of insufficient oxygen supply in high-altitude regions, which is widely present in plateau areas around the world [1–4]. High-altitude hypoxia can lead to a series of physiological and pathological changes, including alterations in cardiovascular, pulmonary, and renal functions, as well as damage to the intestinal mucosal barrier [3,5]. In particular, the damage to the intestinal mucosal barrier can cause pathological processes such as intestinal inflammation and bacterial translocation [5,6].

Macrophage (Mψ) are important components of the immune system, participating in tissue inflammatory responses and innate immune reactions [7–9]. Previous studies have found that Mψ play a crucial role in maintaining the intestinal mucosal barrier [10–12]. Research also indicates that Mψ in organisms with varying hypoxia tolerance exhibit distinct molecular biological characteristics. Specifically, in hypoxia-susceptible animals, Mψ show a particular tendency towards pro-inflammatory polarization [13]. However, under high-altitude hypoxia conditions, the function and metabolic state of Mψ may be affected, and whether this is involved in the molecular mechanisms of intrinsic mucosal barrier injury caused by high-altitude hypoxia remains to be further investigated [14–16].

Glycolysis metabolism is one of the important metabolic pathways for cell survival and function maintenance, playing a vital role in Mψ polarization and functional regulation [17,18]. However, it is currently unclear whether Mψ participate in the regulation of intrinsic mucosal barrier injury caused by high-altitude hypoxia through the modulation of glycolysis metabolism [19–21]. Firmicutes are considered to be an important group of bacteria in high-altitude environments. Therefore, it has significant scientific significance to investigate whether firmicutes mediate Mψ polarization by modulating glycolysis metabolism and thus participate in the molecular mechanisms of intrinsic mucosal barrier injury [22–24].

The molecular mechanisms were explored using single-cell transcriptome sequencing and metabolomics analysis in this study. A high-altitude hypoxia mouse model was employed to identify key cell types involved in regulating intrinsic mucosal barrier injury caused by high-altitude hypoxia through single-cell transcriptome sequencing analysis [25,26]. Furthermore, metabolomics analysis of colon tissue Mψ and assessment of Mψ metabolites were conducted to elucidate the pivotal proteins and metabolic pathways influencing the barrier injury [27–29]. Mechanistic validation was performed using mouse Mψ RAW264.7 cells *in vitro* and by transplanting firmicutes intestinal flora in vivo to further investigate the molecular mechanisms [30,31].

The purpose of this study is to reveal whether firmicutes mediate Mψ polarization through the HIF-1α-mediated glycolysis pathway, thus alleviating intrinsic mucosal barrier injury caused by high-altitude hypoxia. This study extensively investigates the relationship between metabolic reprogramming in Mψ and intrinsic mucosal barrier injury induced by high-altitude hypoxia, providing new molecular mechanisms for understanding the pathological processes associated with high-altitude hypoxia. Moreover, the findings of this study are expected to provide scientific evidence for the development of therapeutic strategies to improve the health of residents in high-altitude regions, which is of great clinical significance.

2. Materials and methods

2.1. Construction and grouping of a mouse model for high-altitude hypoxia

Fifty healthy male C57BL/6J mice aged 4–6 weeks were purchased from Charles River, China (219). The mice were individually housed in SPF-grade animal facilities with humidity maintained at 60%–65 % and temperature controlled at 22–25 °C. They were subjected to a 12-h light-dark cycle and provided ad libitum access to food and water. Following a one-week adaptation period, the mice's health status was monitored. To simulate an environment at an altitude of 3500–4000 m inside a low-pressure oxygen chamber, the mice were exposed to continuous hypoxia for 14 days with the pressure set at 60–65 kPa. Prior to sample collection, the mice underwent a 12-h fast and were euthanized with 100 mg/kg pentobarbital sodium (11715, Merck, USA) via eye blood collection. The entire colon tissues were then extracted. A control group underwent the same experimental interventions in a plain environment [32]. The control group consisted of 12 mice, while the experimental group comprised 38 mice (36 for experiments and 2 as backups). For single-cell sequencing experiments, 2 mice from each of the control and experimental groups were used; for quantitative proteomics analysis, 4 mice from each group were used; and for metabolomics analysis, 6 mice from each group were used. In the in vivo experiments using the high-altitude hypoxic mouse model, the experimental mice were divided into four groups with 6 mice in each group: LV-NC (mice transfected with empty vector), LV-NC + FMT (mice transfected with empty vector and subjected to fecal microbiota transplantation), LV-HIF-1α (mice transfected with HIF-1α vector), and LV-HIF-1α+FMT (mice transfected with HIF-1α vector and subjected to fecal microbiota transplantation).

All mice were raised in a specific pathogen-free (SPF) environment and provided with sterilized feed and water. In accordance with

the "Guide for the Care and Use of Laboratory Animals" written by the National Academy of Sciences and published by the National Institutes of Health, humane care was provided to all animals in accordance with the established standards. This experimental protocol and the use of animals were approved by our institution's ethics committee [32].

Prior to modeling, an LV-HIF-1α vector was constructed, and the same procedure was performed to distribute it into the cells. The vector was injected into the mice through the tail vein at a concentration of MOI = 10, with a working titer of approximately 5×10^6 TU/mL. Each injection was 100 μL, twice a week, for a duration of 2 weeks [33].

In conducting fecal microbiota transplantation, we obtained a bacterial solution from the feces of healthy male C57BL/6 mice weighing between 18 and 22 g. This solution contained a high concentration of bacteria cells from the Firmicutes phylum. Numerous studies have indicated that Firmicutes bacteria are predominant in the feces of healthy mice, constituting over 60 % of the fecal bacterial solution [34,35]. We hypothesized in our study that Firmicutes bacteria played a pivotal role in the feces of healthy mice and investigated their effects using fecal microbiota transplantation from healthy mice. The mice were fed a standard laboratory diet and tap water. During the modeling phase, the new bacterial solution was aliquoted into 1.5 mL EP tubes using a gavage tube method. Mice were administered 0.3 mL of the fecal bacterial solution daily for 14 days [34].

2.2. H&E staining

The mouse colon tissue was stained using the H&E staining kit (C0105, Beyotime, China). The procedure was as follows: first, the mouse colon tissue was fixed in 10 % neutral buffered formalin at 4 °C for 24 h. Then, it underwent dehydration, embedding in paraffin, and sectioning. The sections were subjected to routine deparaffinization with xylene, gradient alcohol hydration, and distilled water rinse. Subsequently, they were stained with hematoxylin for 5–10 min. The excess staining solution was washed off with deionized water for approximately 10 min, followed by staining with eosin for 30 s to 2 min. Afterward, the sections were dehydrated with gradient alcohol and cleared with xylene. Finally, neutral gum or other mounting mediums were used to mount the sections, and observation and photography were performed under an inverted microscope (IX73, Olympus, Japan) [6]. Please refer to Table S1 for the scoring criteria.

2.3. Pimonidazole staining

After fixation, dehydration, and trimming of the colon tissue, it was embedded in paraffin. Once the sections were prepared, deparaffinization was carried out until water and endogenous peroxidase in the tissue were quenched with a buffer solution. Then, the tissue was washed twice with buffer solution and placed in a target retrieval reagent. Antigen retrieval was performed at 90 °C for 20 min. After cooling to room temperature, the tissue was washed twice with a buffer solution. Next, a protein-blocking agent was added to block background staining. The HypoxyprobeTM-1 Plus Kit (HP1-1000Kit, Hypoxyprobe, USA) was used to detect hypoxia in the mouse colon tissue. First, the tissue was incubated with FITC-conjugated mouse IgG1 monoclonal antibody from the kit at room temperature for 60 min, followed by two washes with buffer solution. Then, rabbit anti-FITC conjugated to horseradish peroxidase, also from the kit, was added and incubated at room temperature for 30 min, followed by two washes with buffer solution. Finally, DAB was used to stop the color development, and the sections were counterstained, dehydrated with alcohol, cleared, and mounted. Panoramic scanning of fluorescence images was performed using a fluorescence microscope (BX53, Olympus, Japan), and the fluorescent area/DAPI fluorescent area was calculated. Each group consisted of 6 mice, with 5 slices from each mouse, and 6–10 fields were randomly observed [6].

2.4. Measurement of reactive oxygen species (ROS)

Colon tissue was fixed, dehydrated, and trimmed before being embedded in paraffin and sectioned. After dewaxing the sections in water, endogenous hydrogen peroxide was quenched using a tissue-specific enzyme and washed twice with a buffer solution. Subsequently, the samples were incubated in target retrieval reagent, removed after 20 min of incubation at 90 °C, and washed twice with buffer solution at room temperature. A protein-blocking agent was added to prevent background staining, followed by the addition of a self-quenching fluorescent dye. Then, staining was performed using ROS dye (D7008, Sigma-Aldrich) and DAPI (32670, Sigma-Aldrich). Finally, the results were observed using a fluorescence microscope (BX53, Olympus, Japan), and images were captured [36].

2.5. Immunohistochemistry experiment

Colon tissue samples were fixed in 4 % paraformaldehyde, dehydrated, cleared, infiltrated with paraffin, and embedded before sectioning. For immunohistochemical staining, the sections were dewaxed and rehydrated, followed by antigen retrieval. The sections were placed in a container containing PBS and heated in a microwave until boiling. Then, staining was performed using a universal immunohistochemistry detection kit (PK10009, Protein Tech, USA) according to the manufacturer's instructions. The primary antibodies used were rabbit anti-Occludin (ab216327, 1:200, Abcam, USA), Claudin-1 (ab307692, 1:200, Abcam, USA), and ZO-1 (ab221547, 1:200, Abcam, USA). Subsequently, 50–100 μL of anti-rabbit HRP-conjugated polymer was added and incubated at room temperature for 30 min. The sections were stained using DAB, counterstained with hematoxylin for 2–3 min, and then rinsed with distilled water. The stained sections were observed and saved using an optical microscope (CX43, OLYMPUS, Japan). A positive area displayed a light brown or tan staining result. Each group consisted of 6 mice with 5 sections per mouse. 6–10 fields were randomly observed to record the number of positive cells. Analysis was performed using an image analysis system (Aperio Scanscope

System, Vista, CA) [32].

2.6. Quantitative detection of FITC-dextran

Before the experiment, mice were fasted for 12 h. FITC-Dextran was dissolved in sterile water for injection. Four hours prior to the experiment, mice were orally administered FITC-Dextran (68059, 4 mg/kg, Sigma-Aldrich) via gavage. After a 4-h water restriction, blood samples were collected from the eye sockets, and fluorescence values were measured using a microplate reader (N50, IMPLEN, Germany) with an excitation wavelength of 485 nm and an emission wavelength of 520 nm. Quantitative analysis was performed based on the calibration curve of FITC-Dextran concentrations in serum [6].

2.7. RT-qPCR

Total RNA from cells and tissues was extracted using TRIzol (15596026, ThermoFisher, USA), and the concentration and purity of the extracted RNA were measured using a nanodrop2000 UV–Vis spectrophotometer (ThermoFisher, USA). The RNA was reverse transcribed into cDNA according to the instructions of the PrimeScript RT reagent Kit (RR047A, Takara, Japan), and RT-PCR was performed using the Fast SYBR Green PCR master mix (11736059, ThermoFisher, USA). Each well was set up in triplicate, and β-actin was used as the internal reference. The relative expression levels were calculated using the $2^{-\Delta\Delta Ct}$ method [37]. The experiment was repeated three times. The primer sequences used for RT-qPCR in this study are listed in Table S2.

2.8. ELISA

An enzyme-linked immunosorbent assay (ELISA) was performed using culture cell supernatant and mouse serum. Mouse IL-1β, IL-6, TNF-α, IL-10, and TGF-β levels were measured in the cell supernatant and mouse serum samples using commercially available ELISA kits: mouse IL-1β ELISA kit (ab197742, Abcam, USA) mouse IL-6 ELISA kit (ab222503, Abcam, USA), mouse TNF-α ELISA kit (ab208348, Abcam, USA), mouse IL-10 ELISA kit (ab255729, Abcam, USA), and mouse TGF-β ELISA kit (ab119557, Abcam, USA) [38]. Each experiment was repeated thrice for each group.

2.9. Single-cell transcriptome sequencing (scRNA-seq)

Colon tissues from normoxic mice (n = 2) and high-altitude hypoxia (n = 2) mice were collected and processed into single-cell suspensions using trypsin (9002-07-7, Sigma-Aldrich, USA). Individual cells were captured using the C1 Single-Cell Auto Prep System (Fluidigm, Inc., South San Francisco, California, USA). Following cell capture, cells were lysed within the chip to release mRNA and reverse-transcribed into cDNA. The lysed and reverse-transcribed cDNA was pre-amplified in a microfluidic chip for subsequent sequencing. The pre-amplified cDNA was then used to construct libraries and subjected to single-cell sequencing on the HiSeq 4000 Illumina platform (sequencing parameters: paired-end reads, read length of 2x75 bp, approximately 20,000 reads per cell) [39].

Data analysis was performed using the "Seurat" package in the R software. Cells were quality-controlled based on the criteria of nFeature_RNA ranging from 200 to 5000 percent.mt being less than 20 % [40]. The top 2000 genes with the highest expression variability were selected as variable genes. Principal Component Analysis (PCA) was performed using these variable genes to reduce the dimensionality of the scRNA-Seq dataset. The first 20 principal components were chosen for downstream analysis using the Elbowplot function in the Seurat package. FindClusters function, provided by Seurat, was used to identify major cell subpopulations with the default resolution (res = 1). Then, the t-SNE algorithm was employed to reduce the non-linear dimensionality of the scRNA-seq sequencing data. The seurat package was used to identify marker genes for various cell subpopulations, and cell annotation was performed using the "Singel R″ package [41].

Differentially expressed genes (DEGs) in the scRNA-Seq dataset were identified using the "Limma" package in R software, with the filtering criteria of $|\log2FC| > 0.5$ and $P < 0.05$. DEGs between normoxic and hypoxic colonic cells were determined [42]. The clusterProfiler package in R was used to perform functional enrichment analysis of co-expressed genes, including Gene Ontology (GO) and Kyoto Encyclopedia of Genes and Genomes (KEGG) pathways, and visualization analysis of data was conducted using the ggplot2 package [43].

2.10. Quantitative proteomic analysis

Mψ from colon tissue were collected from normoxia mice (n = 4) and high-altitude hypoxia mice (n = 4). RIPA buffer containing proteinase inhibitors was used to extract Mψ proteins. During the extraction process, samples were treated with an ultrasonic instrument for 30 s every 5 min, three times in total, to ensure complete cell rupture and protein release. The concentration of the extracted protein samples was determined using the BCA protein quantification kit, and the concentration of each sample was ensured to be within an acceptable range based on the standard curve. After adjusting the pH to 8.0, trypsin was added to the samples at a ratio of 1:50 (enzyme to protein) for 16 h of enzymatic digestion at 37 °C. The digested samples were then subjected to ZipTip C18 clean-up and loaded onto a high-performance liquid chromatography system connected to a mass spectrometer for MS/MS analysis. The MaxQuant software was used for data processing, including protein identification and quantification.

Desalted peptides labeled with 0.1 % formic acid (FA) were used for iTRAQ labeling and mass spectrometry analysis. Each sample was analyzed three times using QSTAR Elite Hybrid MS (Applied Biosystems/MDS-SCIEX) and an online HPLC system (Shimadzu,

Japan). In each analysis, 30 μl of peptide solution was injected and separated on a homemade nano-column with a C18 stationary phase. The column outlet was equipped with a micro-flow nano-electrospray source (75 μm ID × 15 cm, 5 μm particles) (New Objectives, Woburn, MA). A 90-min high-performance liquid chromatography gradient was established using mobile phase A (0.1 % FA/2 % ACN) and mobile phase B (0.1 % FA/100 % ACN), with an effective flow rate of 0.2 μl/min. The mass flow rate was set to 30 μl/min using a splitter. The mass spectrometer was operated in positive ion mode for data acquisition. Precursors with a charge of +2 to +4 in the mass range of 300–2000 *m/z* were selected for fragmentation. In each MS/MS spectrum, the three most abundant peptide ions with a count threshold exceeding 5 were selected. The dynamic exclusion time for selected precursor ions was set to 30 s, and the mass tolerance was set to 30 mDa. Automated collision energy and automated spectral/mass spectral accumulation were used for data-dependent acquisition. The fragment intensity multiplier was set to 20, and the maximum accumulation time was set to 2 s. Three LC-MS/MS injections (technical replicates = 3) were performed for better coverage and statistical consistency of the target proteome. Western blot analysis was used for protein validation of the same sample after proteomic analysis. The parameters were: (1) MS: scan range (*m/z*) = 350–1500; resolution = 120,000; AGC target = 4e5; maximum injection time = 50 ms; (2) HCD-MS/MS: resolution = 30,000; AGC target = 1e5; collision energy = 33; (3) DIA (data-independent acquisition). Each window overlapped by 1 *m/z*, and there were a total of 47 windows. The iRT kit (Ki3002, Biognosys AG, Switzerland) was added to calibrate the retention time of the extracted peptide peaks. The DIA dataset was generated using Spectronaut V13 (Biognosys AG, Switzerland), including data normalization and relative protein quantification. The differentially expressed proteins were filtered using Welch's ANOVA test with a significance level of $P < 0.05$ and a fold change greater than 1.0 in absolute value [44].

2.11. Metabolomic analysis

Mψ were collected from the colon tissues of normoxic mice (n = 6) and high-altitude hypoxia mice (n = 6). Each sample was transferred to a 1.5 mL polypropylene tube with 300 μL in each. Then, it was mixed with 900 μL of 80 % methanol and 0.1 % formic acid and centrifuged at 12,000 g for 10 min after vortexing for 2 min. The supernatant was transferred to a vial in an auto-sampler.

Blood plasma metabolomic analysis was performed using an LC20 ultra-high-performance liquid chromatography system (Shimadzu, Japan) combined with a Triple TOF-6600 mass spectrometer (AB Sciex). Chromatographic analysis was conducted using a Waters ACQUITY UPLC HSS T3 C18 (100 × 2.1 mm, 1.8 μm) column. The column temperature was maintained at 40 °C, and elution was carried out at a flow rate of 0.4 mL/min. The mobile phase consisted of an acetonitrile-water solution containing 0.1 % formic acid. The gradient elution program for mobile phase B was as follows: 5 %, 0.0–11.0 min; 90 %, 11.0–12.0 min; 5 %, 12.1–14 min. The eluate was directly introduced to the mass spectrometer without splitting [45].

The mass spectrometry conditions were as follows: ionization voltage of 5500 V; capillary temperature of 550 °C; spray gas flow rate of 50 psi; auxiliary heating gas flow rate of 60 psi. Orthogonal partial least squares-discriminant analysis (OPLS-DA) and permutation test (100 permutations) were performed on the preprocessed data to avoid overfitting. Metabolites with VIP scores >1 and p-values <0.05 in the OPLS-DA model were identified as differentially expressed metabolites (DMs). Additionally, metabolites with fold changes ≥2 and ≤ 0.5 and p-values <0.05 in the Student's t-test were selected as the final set of differentially expressed metabolites. MetaboAnalyst (Version 5.0) was utilized to identify relevant metabolic pathways [46].

2.12. Establishment of a hypoxia cell model and transfection of cell groups

To establish the hypoxia cell model, RAW264.7 cells, a mouse Mψ cell line (TIB-71, ATCC, USA), were cultured in Dulbecco's Modified Eagle Medium (DMEM) supplemented with 10 % heat-inactivated fetal bovine serum (FBS) at 37 °C in a humidified atmosphere containing 5 % CO_2. For the hypoxia experiment, cells were cultured under an anaerobic system (1 % O_2, 5 % CO_2, 94 % N_2) for 48 h, while the control group cells were cultured under normal oxygen tension (20 % O_2, 5 % CO_2) [47].

The LV-HIF-1α vector was constructed by Genechem (Shanghai) and packaged into lentiviruses. The lentiviral vector for overexpressing HIF-1α was named LV-HIF-1α. When the cells reached the logarithmic growth phase, they were trypsinized, resuspended in a cell suspension with a density of 5×10^4 cells/mL, and seeded in a 6-well plate at a volume of 2 mL per well. Before LPS stimulation, each lentivirus was added to the cell culture medium at an MOI of 10 (viral titer: 1×10^8 TU/mL) and incubated for 48 h. Stable cell strains were selected using 2 μg/mL puromycin (Catalog No: UC0E03, Sigma-Aldrich, Germany) for two weeks [48–51].

2-DG (2-Deoxy-D-glucose)(HY-13966, MedChemexpress, USA) is an inhibitor of the glycolytic pathway. In this experiment, the concentration of 2-DG used was 16 mM, and cells were treated for 48 h [52]. The cells were divided into nine groups, as specified in Table S3.

2.13. CCK-8 assay

We used the CCK-8 assay kit (C0038, Beyotime Biotechnology, China) to measure the inhibitory effect of different concentrations of butyric acid (B103500, Sigma, USA), secondary bile acid (D2510, Sigma, USA), and lactic acid (1356734, Sigma, USA) on RAW264.7 cells. The inhibitory rate was calculated using the following formula: Inhibitory rate = [OD(DEME) - OD(treated)]/[OD(DEME) - OD(blank)] × 100 %. After culturing the cells under hypoxic conditions for 48 h, we digested the cells and suspended them in L15 and MEM culture media separately. Then, we seeded the cells in a concentration of 3×10^3 cells/well in a 96-well plate. After 48 h of incubation, we measured the absorbance values to assess cell viability. In each well, we added 10 μL of CCK-8 solution and incubated it at 37 °C for 2 h. Subsequently, we used a microplate reader (A51119500C, ThermoFisher, USA) to measure the absorbance at 450 nm [53,54]. Each experiment was performed in triplicate.

2.14. Western blot

RAW264.7 cells and colon tissue were lysed in RIPA lysis buffer (P0013B, Beyotime Biotechnology, China). Protein concentration was quantified using the BCA method (A53226, Thermo Fisher Scientific, USA). Protein samples were separated by SDS-PAGE and transferred to a PVDF membrane (PVH85R, Millipore, Germany) using the wet transfer method. The membrane was then blocked for 1 h at room temperature with 5 % BSA. Subsequently, the membrane was incubated overnight at 4 °C with primary antibodies, including rabbit anti-HIF-1α (ab308433, 1:1000), rabbit anti-GCK (ab88056, 1:1000), rabbit anti-PFK (ab154804, 1:1000), rabbit anti-PKM (ab150377, 1:1000), rabbit anti-LDHA (ab52488, 1:1000) and rabbit anti-β-actin (ab8227, 1:1000). After washes, the membrane was incubated for 2 h with HRP-conjugated goat anti-rabbit IgG secondary antibody (ab6721, 1:5000). Following three 5-min washes with TBST, chemiluminescence was detected. Protein quantification analysis was performed using ImageJ software by calculating the ratio of the grayscale value of each protein to either β-actin or the corresponding unphosphorylated protein [55]. Each experiment was repeated three times.

2.15. Cellular metabolism measurement

Glucose Consumption: The supernatant from RAW264.7 cells was collected and placed in 10 mL centrifuge tubes. The glucose consumption of different cell groups was determined using a glucose assay kit (F006-1-1, Nanjing Jiancheng Bioengineering Institute, China). The glucose concentration in each sample culture medium was calculated by subtracting the glucose concentration in the original high-glucose culture medium, indicating the level of consumption [56].

Acetate and LDH Levels: Cultured RAW264.7 cells were collected, and the levels of acetate and LDH in the cells were measured using an acetate assay kit (A081-1-1, Nanjing Jiancheng Bioengineering Institute, China) and an LDH assay kit (A020-2-2, Nanjing Jiancheng Bioengineering Institute, China), respectively [57].

2.16. Glucose uptake

RAW264.7 cells were seeded in a 24-well plate at a density of 1×10^6 cells/mL. The glucose uptake ability of RAW264.7 cells was assessed using the 2-NBDG Glucose Uptake Assay Kit (ab287845, Abcam, USA). The cells were washed twice with PBS to remove residual 2-NBDG. Immunofluorescence analysis was then performed to evaluate the uptake of 2-NBDG [58].

2.17. Immunofluorescence staining

RAW264.7 cells and colon tissues were fixed with 4 % paraformaldehyde at room temperature for 15 min. After two washes with PBS, permeabilization was done using 0.5 % Triton X-100 (P0096, Beyotime Biotechnology, China) for 10 min. Subsequently, the cells and tissues were incubated with the following primary antibodies: rabbit anti-PKM (ab150377, 1:50), rabbit anti-iNOS (ab178945, 1:500), rabbit anti-ARG1 (ab96183, 1:100), rabbit anti-HIF-1α (ab308433, 1:100), mouse anti-LDHA (66287-1-IG, 1:100), and mouse anti-CD68 (65187-1-IG, 1:100) overnight at 4 °C. After the incubation, the sections were washed three times with PBS and then incubated with either goat anti-rabbit Alexa Fluor 647 (ab150083, 1:200) or goat anti-rabbit Alexa Fluor 488-conjugated secondary antibody (ab150077, 1:200), or goat anti-mouse Alexa Fluor 647 (ab150115, 1:200) or goat anti-rabbit Alexa Fluor 488-conjugated secondary antibody (ab150113, 1:200) for 1 h at room temperature. Subsequently, the sections were washed three times with PBS and stained with DAPI (D3571, 10 μg/mL) for 10 min. The sections were stored at 4 °C and observed under a fluorescence microscope (IMT-2, Olympus, Japan). The protein fluorescence area/DAPI fluorescence area was calculated using ImageJ software. For cell experiments, 5 sections were taken per cell, and 6–10 fields were randomly observed for each experiment group, with 3 experimental repetitions. For animal experiments, 6 mice were included in each group, and 5 sections were taken per mouse. 6–10 fields were randomly observed. All antibodies, except for LDHA and CD68, were purchased from Abcam [59].

2.18. Flow cytometry

RAW264.7 cells and colon tissue were treated with 0.25 % trypsin (25200072, Gibco, USA) and subsequently counted. Approximately 1×10^6 cells were resuspended in 200 μL of fluorescence-activated cell sorting (FACS) buffer (660585, BD Biosciences, USA), and 2 μL of fluorescent antibodies and isotype controls were added. The cells were incubated on ice for 30 min. Next, BMSCs were washed with FACS buffer, fixed with 10 % formalin (R04587, Merck, USA), and subjected to antigen positivity measurement using a BD FACSCalibur flow cytometer (BD Biosciences, USA). Antibodies used were CD80 (ab307467, 1:500, Abcam, USA) and CD206 (MA5-16871, 1:20, Invitrogen, USA) [60].

2.19. Statistical analysis

The statistical analysis of the data in this study was conducted using IBM SPSS software (version 21.0, IBM, USA). Descriptive statistics were presented as the mean ± standard deviation. Prior to analysis, normality and homogeneity of variance were verified. When the data met the assumptions of normal distribution and homogeneity of variance, an independent samples *t*-test was employed to compare differences between two groups, while one-way analysis of variance (ANOVA) or repeated measures ANOVA was used to compare differences among multiple groups. In cases where the data did not follow a normal distribution, non-parametric tests such as

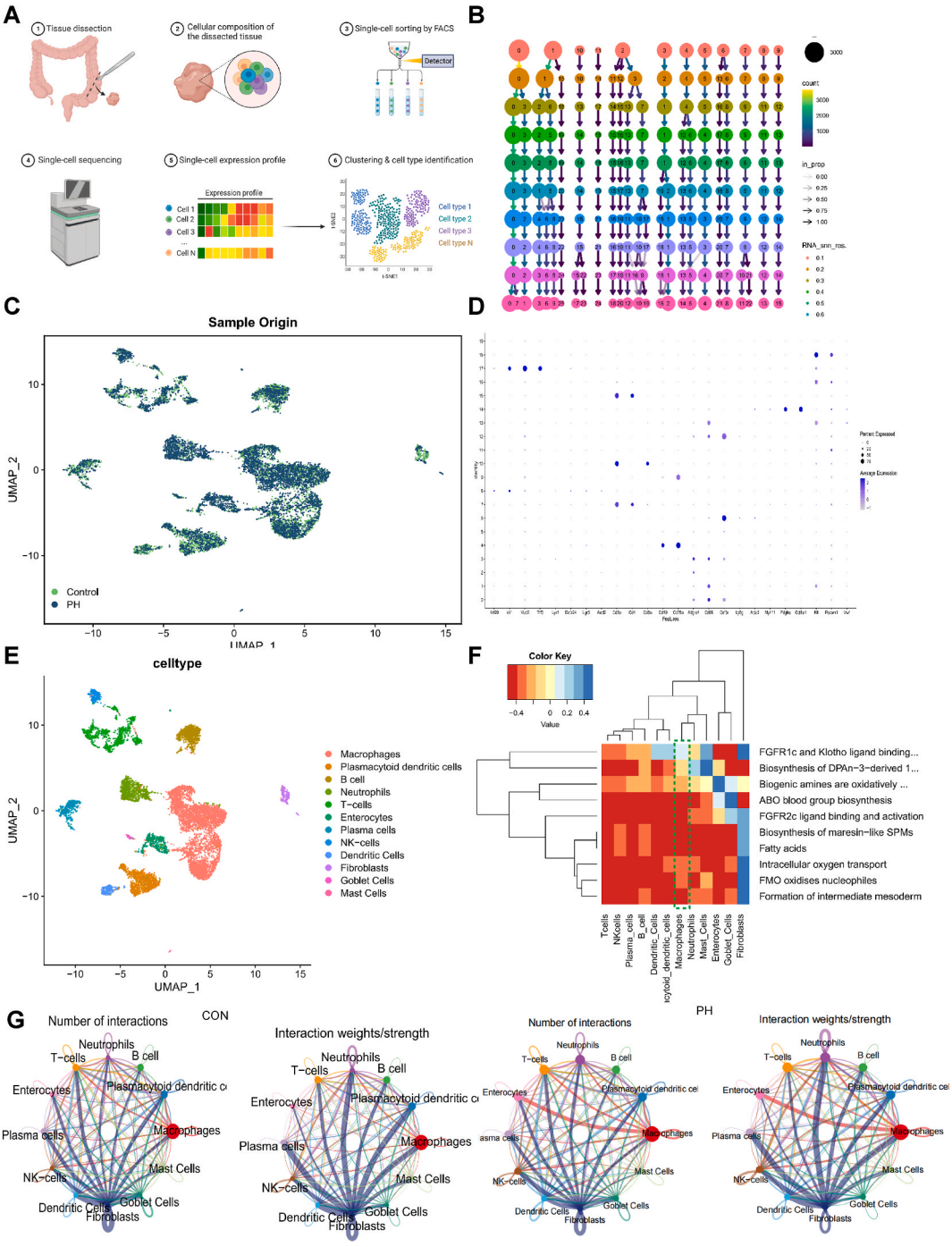

Fig. 1. Quality control, filtering, and principal component analysis of scRNA-seq data. Note: (A) Single-cell sequencing workflow for CON and PH groups; (B) Clustering plot of sample data after batch correction using the harmony package; (C) Two-dimensional scatter plot generated by UMAP algorithm, showing the distribution of cells in CON and PH groups; (D) Heatmap of protein markers associated with each cell cluster; (E) Visualization of cell annotation results based on UMAP clustering; (F) Heatmap of DEGs and cells based on pathway enrichment analysis; (G) Display of interaction frequency and intensity between cells of CON and PH groups.

Kruskal-Wallis and Dunn tests were utilized for statistical comparisons. A significance level of $P < 0.05$ was considered statistically significant.

3. Results

3.1. High-altitude hypoxia induces Mψ-mediated intestinal mucosal barrier injury

First, we established a mouse model of high-altitude hypoxia-induced intestinal mucosal barrier injury (Fig. S1A). We performed multiple tests and analyses on the colon tissues of the control (CON) group and high-altitude hypoxia (PH) group, including histological examination, pimonidazole staining, ROS measurement, immunohistochemistry, FITC-D4 permeability, RT-qPCR, and ELISA.

The results of H&E staining showed that the colon tissue of the CON group had a normal morphology with well-arranged epithelial cells and tight cell arrangement. In contrast, the colon tissue of the PH group showed increased crypt spacing, crypt hyperplasia, disordered intestinal gland arrangement, and inflammatory infiltration in the lamina propria (Fig. S1B). Pimonidazole staining, indicating hypoxia, showed significantly increased green fluorescence in the colon tissue of the PH group compared to the CON group (Fig. S1C). ROS measurement revealed significantly increased red fluorescence in the colon tissue of the PH group compared to the CON group (Fig. S1D). Immunohistochemistry showed significant downregulation of Claudin-1, Occludin, and ZO-1 protein expression in the colon tissue of the PH group compared to the CON group (Fig. S1E). FITC-D4 permeability assay indicated significantly increased permeability in the colon tissue of the PH group compared to the CON group (Fig. S1F). RT-qPCR demonstrated significantly upregulated mRNA expression levels of IL-1β, IL-6, and TNFα in the colon tissue of the PH group compared to the CON group (Fig. S1G). ELISA revealed significantly increased levels of IL-1β, IL-6, and TNFα in the serum of the PH group mice compared to the CON group

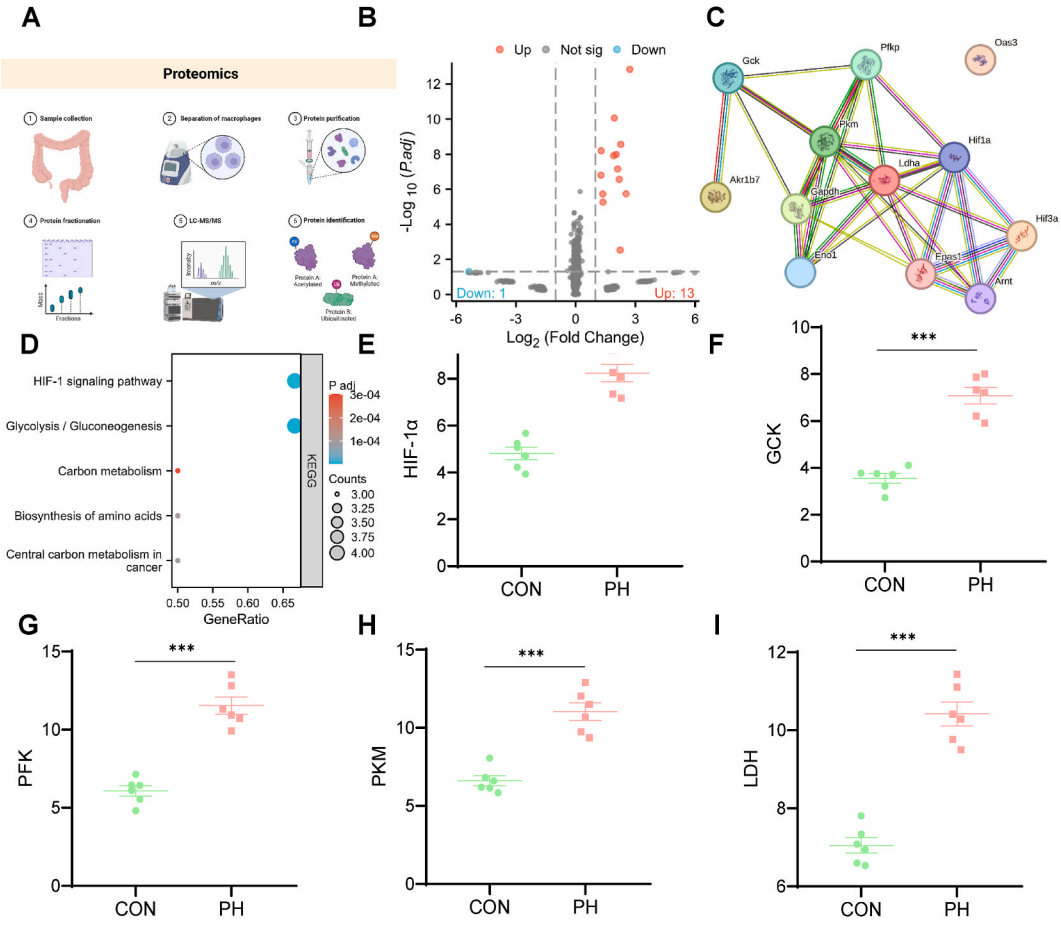

Fig. 2. Proteomic analysis of CON and PH groups. Note: (A) Proteomic workflow for CON and PH groups; (B) Volcano plot showing differential proteins in intestinal tissue samples of CON and PH groups; (C) Intersection of PPI networks constructed from 14 DEGs; (D) KEGG pathway enrichment analysis of the 14 DEGs; (E) Comparison of HIF-1α protein expression between CON and PH groups; (F) Comparison of GCK protein expression between CON and PH groups; (G) Comparison of PFK protein expression between CON and PH groups; (H) Comparison of PKM protein expression between CON and PH groups; (I) Comparison of LDHA protein expression between CON and PH groups. Each group consisted of 4 mice, and the values are presented as mean ± standard deviation. *** indicates $P < 0.001$.

(Fig. S1H).

In conclusion, the above results demonstrate that high-altitude hypoxia leads to changes in colon cell morphology, inflammatory cell infiltration, disruption of the lamina propria, and impairment of the intestinal mucosal barrier.

To elucidate the molecular mechanisms underlying high-altitude hypoxia-induced intestinal mucosal barrier injury, we collected colon tissue from normoxic mice (CON) and high-altitude hypoxia mice (PH) for scRNA-seq. We applied the Seurat package to integrate and initially check the quality of the scRNA-seq data, including the number of genes per cell (nFeature_RNA), the number of mRNA molecules per cell (nCount_RNA), and the percentage of mitochondrial genes (percent.mt). The results showed that most cells had nFeature_RNA less than 5000, nCount_RNA less than 20000, and percent.mt less than 20 % (Fig. S2A). The correlation analysis of sequencing depth indicated a correlation coefficient of −0.11 between nCount_RNA and percent.mt and a correlation coefficient of 0.88 between nCount_RNA and nFeature_RNA in the filtered data (Fig. S2B). This suggests that the filtered cell data has good quality and can be further analyzed.

Next, we conducted further analysis on the filtered cells and selected the top 1500 genes with high expression variance for downstream analysis (Fig. S2C). Cell cycle scoring was performed to assess the cell cycle stage (Fig. S2D), and the data were then normalized. PCA was used for linear dimension reduction. Here, we present a heatmap of the gene expression of the top correlated genes with PC_1 - PC_6 (Fig. S2E) and the distribution of cells in PC_1 and PC_2 (Fig. S2F). The results showed certain batch effects among the samples.

The technical workflow of scRNA-seq analysis is shown in Fig. 1A. To reduce batch effects and improve the accuracy of cell clustering, we applied the harmony package for batch correction. Finally, we obtained the results with a resolution of 0.4 (Fig. 1B).

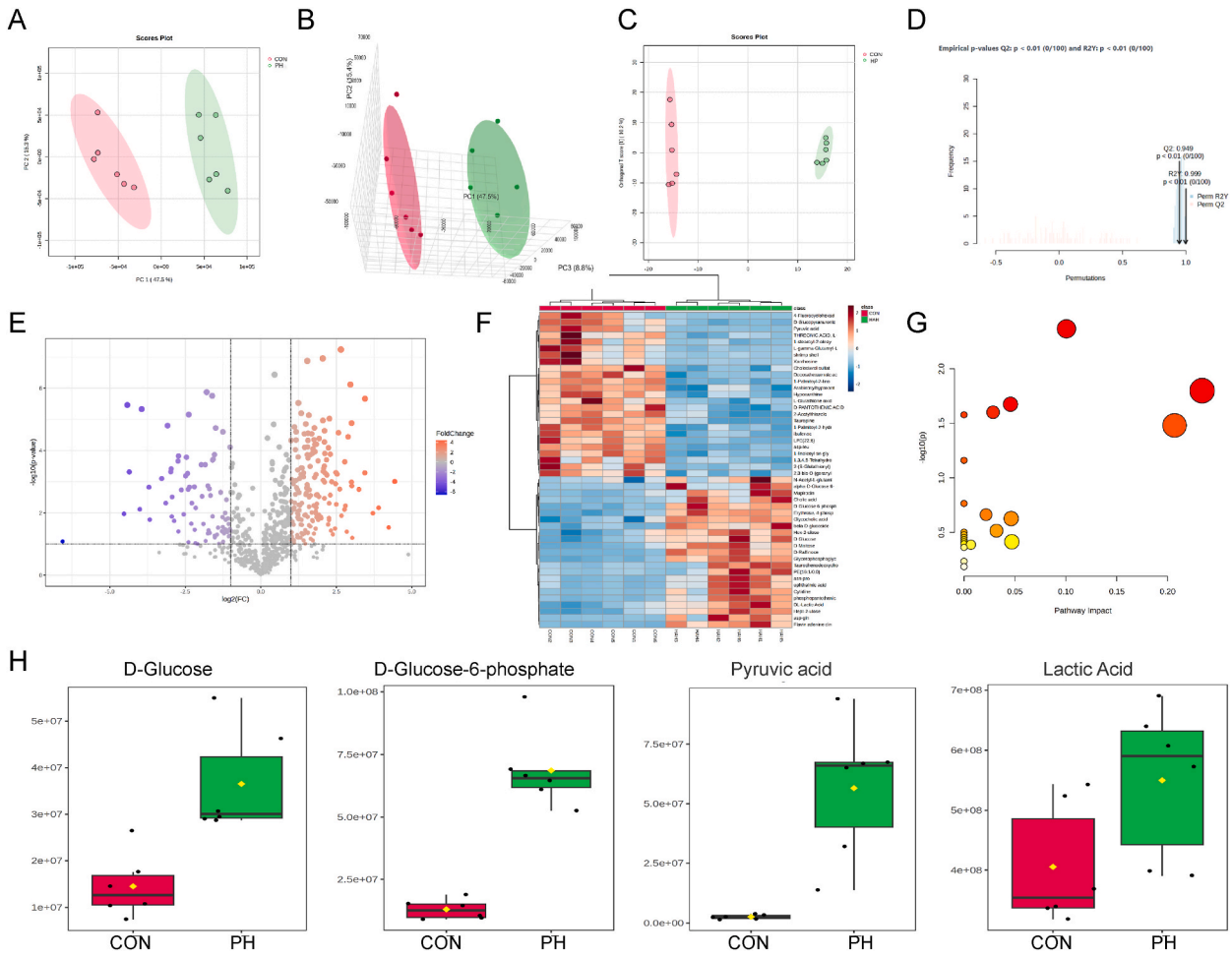

Fig. 3. Untargeted metabolomic analysis of CON and PH groups.

Note: (A) PCA score plot of intestinal tissue samples from CON and PH groups; (B) 3D-PCA score plot of intestinal tissue samples from CON and PH groups; (C) OPLS-DA score plot of intestinal tissue samples from CON and PH groups; (D) Permutation analysis to assess the classification of intestinal tissue samples between CON and PH groups; (E) Volcano plot showing differential metabolites in intestinal tissue samples from CON and PH groups; (F) Heatmap of differential metabolites in intestinal tissue samples from CON and PH groups; (G) KEGG bubble plot of differential metabolites in intestinal tissue samples from CON and PH groups; (H) Peak area of D-Glucose, D-Glucose-6-phosphate, Pyruvic acid, and Lactic Acid in intestinal tissue samples from CON and PH groups.

UMAP algorithm was used for nonlinear dimension reduction of the top 20 principal components. Through UMAP clustering analysis, we generated a two-dimensional scatter plot showing the cell distribution of the CON and PH groups (Fig. 1C), as well as the marker proteins of each cell cluster (Fig. 1D). By scRNA-seq analysis, we successfully identified 12 cell types, including Mψ, plasma cell-like dendritic cells, B cells, neutrophils, T cells, intestinal epithelial cells, plasma cells, NK cells, dendritic cells, fibroblasts, goblet cells, and mast cells (Fig. 1E). Lastly, differential analysis of the cells revealed that the differential genes mainly influenced intracellular oxygen transport, with Mψ showing the most significant effects (Fig. 1F). Furthermore, simulation results using the CellChat package indicated enhanced communication between Mψ and intestinal epithelial cells in the PH group compared to the CON group (Fig. 1G).

In summary, Mψ are key cells in high-altitude hypoxia-induced intestinal mucosal barrier injury.

3.2. Key cells and proteins of Mψ and HIF-1α in high-altitude hypoxia-induced intestinal mucosal barrier injury

Based on single-cell sequencing results, we have found that Mψ are the key cell type responsible for the damage to the intestinal mucosal barrier caused by high-altitude hypoxia. To identify the key proteins involved in the intestinal mucosal barrier injury induced by high-altitude hypoxia, we collected intestinal tissue samples from the CON and PH groups and performed proteomic analysis, as depicted in Fig. 2A. Differential analysis results revealed a total of 14 differentially expressed proteins, of which 13 were upregulated, including GAPDH, PKM, ENO1, LAHA, GCK, PFKC, HIF-1α, HIF-1β, HIF-2α, HIF-2β, HIF3α, and LDHA, while 1 protein, OAS3, was downregulated (Fig. 2B). To further investigate the key proteins associated with high-altitude hypoxia-induced intestinal mucosal barrier injury, these 14 DEGs were analyzed using the String database, with the mouse species as the restriction and a confidence score set to 0.7, to construct a PPI network of the encoded proteins. From the PPI network, we observed that LDHA had a degree of 9 and a confidence score of 0.966667, while HIF-1α had a degree of 8 and a confidence score of 0.9 (Fig. 2C–Table S4). The activation of HIF-1α promotes cells to shift from oxygen-dependent mitochondrial oxidative phosphorylation to glycolysis, which is a more efficient energy generation pathway, particularly under hypoxic conditions [61]. The upregulation of key enzymes involved in glycolysis, such as lactate dehydrogenase and glucokinase, by HIF-1α further supports its central role in regulating cellular metabolism and adaptation to hypoxic conditions [62]. Thus, HIF-1α is a key protein involved in high-altitude hypoxia-induced intestinal mucosal barrier injury. A KEGG enrichment analysis of the 14 DEGs revealed significant enrichment in pathways such as Glycolysis/Gluconeogenesis, HIF-1 signaling pathway, Central carbon metabolism in cancer, and Biosynthesis of amino acids (Fig. 2D). Functional enrichment results indicated that the differentially expressed proteins mainly involved mucosal barrier injury, oxidative stress, and inflammatory responses. KEGG analysis also identified the involvement of differentially expressed proteins in the regulation of glycolysis/gluconeogenesis and the HIF-1 signaling pathway, among other cellular activities. Finally, we presented the expression of key proteins in the HIF-1αand glycolysis (GCK, PFK, PKM, LDHA), as revealed by proteomic analysis. The results demonstrated a significant increase in the protein expression of HIF-1α, GCK, PFK, PKM, and LDHA in the PH group compared to the CON group (Fig. 2E–I).

3.3. High-altitude hypoxia induces intestinal mucosal barrier injury via glycolysis regulation

To further investigate whether high-altitude hypoxia-induced intestinal mucosal barrier injury is regulated by glycolysis, we collected intestinal tissue samples from the CON and PH groups for untargeted metabolomics analysis. The PCA results clearly showed a separation between the CON and PH groups (Fig. 3A and B). Additionally, the OPLS-DA results showed a stable model with a displacement analysis R2Y value of $0.999 > 0.8$, and the OPLS-DA score plot clearly demonstrated the separation between the CON and PH groups (Fig. 3C and D). The differential analysis revealed a total of 48 differentially expressed metabolites between the CON and PH groups, with 24 upregulated and 24 downregulated metabolites (Fig. 3E and F, Table S5). Further enrichment analysis of the differentially expressed metabolites in the KEGG pathway indicated significant enrichment in the glycolysis/gluconeogenesis pathway (Fig. 3G–Table S6). Finally, a comparison of glycolytic metabolites between the CON and PH groups showed higher peak areas of D-Glucose, D-Glucose-6-phosphate, Pyruvic acid, and Lactic Acid in the PH group compared to the CON group (Fig. 3H).

In summary, these findings suggest that high-altitude hypoxia may increase intestinal mucosal barrier injury through the glycolysis pathway.

3.4. HIF-1α regulates Mψ polarization by activating the glycolytic pathway under hypoxic conditions

According to the results of metabolomics analysis, high-altitude hypoxia leads to intestinal mucosal barrier injury in mice Mψ, and HIF-1α is highly expressed and mainly affects the glycolytic pathway. Therefore, we hypothesize that promoting HIF-1α expression and activating the glycolytic pathway under hypoxic conditions could regulate Mψ polarization. 2-DG is a glucose analog that inhibits glycolysis by acting on hexokinase. Consequently, we selected 2-DG as the inhibitor of the glycolytic pathway [63].

Firstly, we validated the effect of HIF-1α on the glycolytic pathway under hypoxic conditions. Western blot analysis revealed that compared to the LV-NC group, the LV-HIF-1α group showed significant upregulation of HIF-1α, GCK, PFK, PKM, and LDH protein expression in cells. The LV-NC+2-DG group showed no significant change in HIF-1α protein expression but significant downregulation of GCK, PFK, PKM, and LDH protein expression. Compared to the LV-HIF-1α group, the LV-HIF-1α+2-DG group showed no significant change in HIF-1α protein expression but significant downregulation of GCK, PFK, PKM, and LDH protein expression (Fig. S3A). ELISA detection results showed that compared to the LV-NC group, the LV-HIF-1α group exhibited a significant increase in glucose consumption, pyruvate, and LDHA content in cells. The LV-NC+2-DG group showed a significant decrease in glucose consumption, pyruvate, and LDHA content. Compared to the LV-HIF-1α group, the LV-HIF-1α+2-DG group showed a significant decrease in glucose consumption, pyruvate, and LDHA content (Fig. S3B). Immunofluorescence detection of cellular glucose uptake revealed that

compared to the LV-NC group, the LV-HIF-1α group exhibited a significant increase in 2-NBDG uptake in cells. The LV-NC+2-DG group showed a significant decrease in 2-NBDG uptake. Compared to the LV-HIF-1α group, the LV-HIF-1α+2-DG group showed a significant decrease in 2-NBDG uptake (Fig. S3C). Immunofluorescence detection of PKM protein expression in cells showed that compared to the LV-NC group, the LV-HIF-1α group exhibited significant upregulation of PKM protein expression. The LV-NC+2-DG group showed significant downregulation of PKM protein expression. Compared to the LV-HIF-1α group, the LV-HIF-1α+2-DG group showed significant downregulation of PKM protein expression (Fig. S3D). These results suggest that overexpression of HIF-1α can activate the glycolytic pathway.

Next, we explored the impact of the HIF-1α/glycolytic pathway on Mψ polarization. Fig. 4A presents the experimental workflow. RT-qPCR analysis demonstrated that compared to the LV-NC group, the LV-HIF-1α group showed significant upregulation in the mRNA levels of M1 Mψ cytokines IL-1β, IL-6, and TNFα and significant downregulation in the mRNA levels of M2 Mψ cytokines IL-10 and TGFβ. Moreover, compared to the LV-NC+2-DG group, the LV-NC group exhibited significant downregulation in IL-1β, IL-6, and TNFα mRNA levels and significant upregulation in IL-10 and TGFβ mRNA levels. Compared to the LV-HIF-1α group, the LV-HIF-1α+2-DG group showed significant downregulation in IL-1β, IL-6, and TNFα mRNA levels and significant upregulation in IL-10 and TGFβ mRNA levels (Fig. 4B).

The results of the flow cytometry analysis showed that the proportion of CD80, a cellular marker for M1 Mψ, was significantly upregulated in the LV-HIF-1α group compared to the LV-NC group. Conversely, the proportion of CD80 was significantly downregulated in the LV-NC+2-DG group compared to the LV-NC group. Moreover, the LV-HIF-1α+2-DG group exhibited a significant decrease in the proportion of CD80 compared to the LV-HIF-1α group (Fig. 4C). Similarly, the proportion of CD206, a cellular marker for M2 Mψ, was significantly downregulated in the LV-HIF-1α group compared to the LV-NC group. In contrast, the LV-NC+2-DG group showed a significant increase in the proportion of CD206 compared to the LV-NC group. Additionally, the LV-HIF-1α+2-DG group exhibited a significant upregulation in the proportion of CD80 compared to the LV-HIF-1α group (Fig. 4D). Furthermore, the expression of iNOS protein was significantly upregulated in the LV-HIF-1α group compared to the LV-NC group, while the LV-NC+2-DG group showed a significant decrease in iNOS protein expression. Compared to the LV-HIF-1α group, the LV-HIF-1α+2-DG group showed downregulation of iNOS protein expression (Fig. 4E). Similarly, the expression of ARG1 protein was significantly downregulated in the LV-HIF-1α group compared to the LV-NC group, whereas the LV-NC+2-DG group exhibited a significant upregulation of ARG1 protein expression. Compared to the LV-HIF-1α group, the LV-HIF-1α+2-DG group showed a significant upregulation of ARG1 protein expression (Fig. 4F). Overall, our results indicate that the overexpression of HIF-1α under hypoxic conditions can activate the glycolytic pathway, thereby promoting M1 Mψ activation and suppressing M2 Mψ polarization.

3.5. *Butyric acid regulates Mψ polarization by inhibiting the HIF-1α/glycolysis pathway*

Butyric acid, secondary bile acids, and lactate are important metabolites of gut microbiota metabolism with a significant impact on intestinal mucosal barrier health and function. Butyric acid serves as a major energy source for colonocytes and plays a crucial role in maintaining the integrity of the intestinal barrier while also exhibiting anti-inflammatory and anticancer properties [64]. Secondary bile acids are conversion products of primary bile acids synthesized in the liver, and they play a key role in maintaining the steady state of the intestinal barrier by interacting with bile acid receptors [65]. Lactate, mainly produced by lactobacilli, not only acts as a byproduct of microbial fermentation but also participates in regulating intestinal barrier function and local immune response [66]. The balance of these metabolites is crucial for gut health, as an imbalance can lead to intestinal mucosal barrier injury and be associated with various intestinal-related diseases.

To further investigate the impact of different gut microbial metabolites on Mψ polarization, we cultured RAW264.7 Mψ under hypoxic conditions for 24 h and subsequently co-cultured them with butyric acid, secondary bile acids, and lactate for an additional 24 h. Firstly, using CCK8, we screened the optimal concentrations of butyric acid, secondary bile acids, and lactate for Mψ, and the results showed that the optimal concentrations were 10 mM for butyric acid and 10 μM for both secondary bile acids and lactate, without any apparent cytotoxicity (Fig. S4A). Next, using RT-qPCR, we found that compared with the PH group, the mRNA levels of M1 Mψ cytokines IL-1β, IL-6, and TNFα were significantly decreased in the butyric acid group, and there was also a reduction in the mRNA levels in both the secondary bile acids and lactate groups, although the effect was more significant in the butyric acid group (Fig. S4B). Flow cytometry results showed that compared with the PH group, the proportion of M1 Mψ marker CD80 was significantly reduced in the butyric acid group, with a similar decrease observed in the secondary bile acids and lactate groups, although the effect was more pronounced in the butyric acid group (Fig. S4C). Compared with the PH group, the proportion of M2 Mψ marker CD206 was significantly increased in the butyric acid group, with a similar increase observed in the secondary bile acids and lactate groups, although the effect was more pronounced in the butyric acid group (Fig. S4D). Lastly, immunofluorescence results showed that compared with the PH group, the protein expression of iNOS was significantly decreased in the butyric acid group, with a similar decrease observed in the secondary bile acids and lactate groups, although the effect was more pronounced in the butyric acid group (Fig. S4E). Compared with the PH group, the protein expression of ARG1 was significantly increased in the butyric acid group, with a similar increase observed in the secondary bile acids and lactate groups, although the effect was more pronounced in the butyric acid group (Fig. S4F).

In conclusion, under hypoxic conditions, butyric acid, secondary bile acids, and lactate can all inhibit the activation of M1 Mψ and promote M2 Mψ polarization. However, butyric acid has a more pronounced inhibitory effect, which is why we chose it for further experimentation.

Next, we investigated the impact of butyric acid, a metabolite produced by gut bacteria, on the HIF-1α/glycolytic pathway. Western blot analysis revealed significant downregulation of HIF-1α, GCK, PFK, PKM, and LDH protein expression in cells treated with LV-NC +

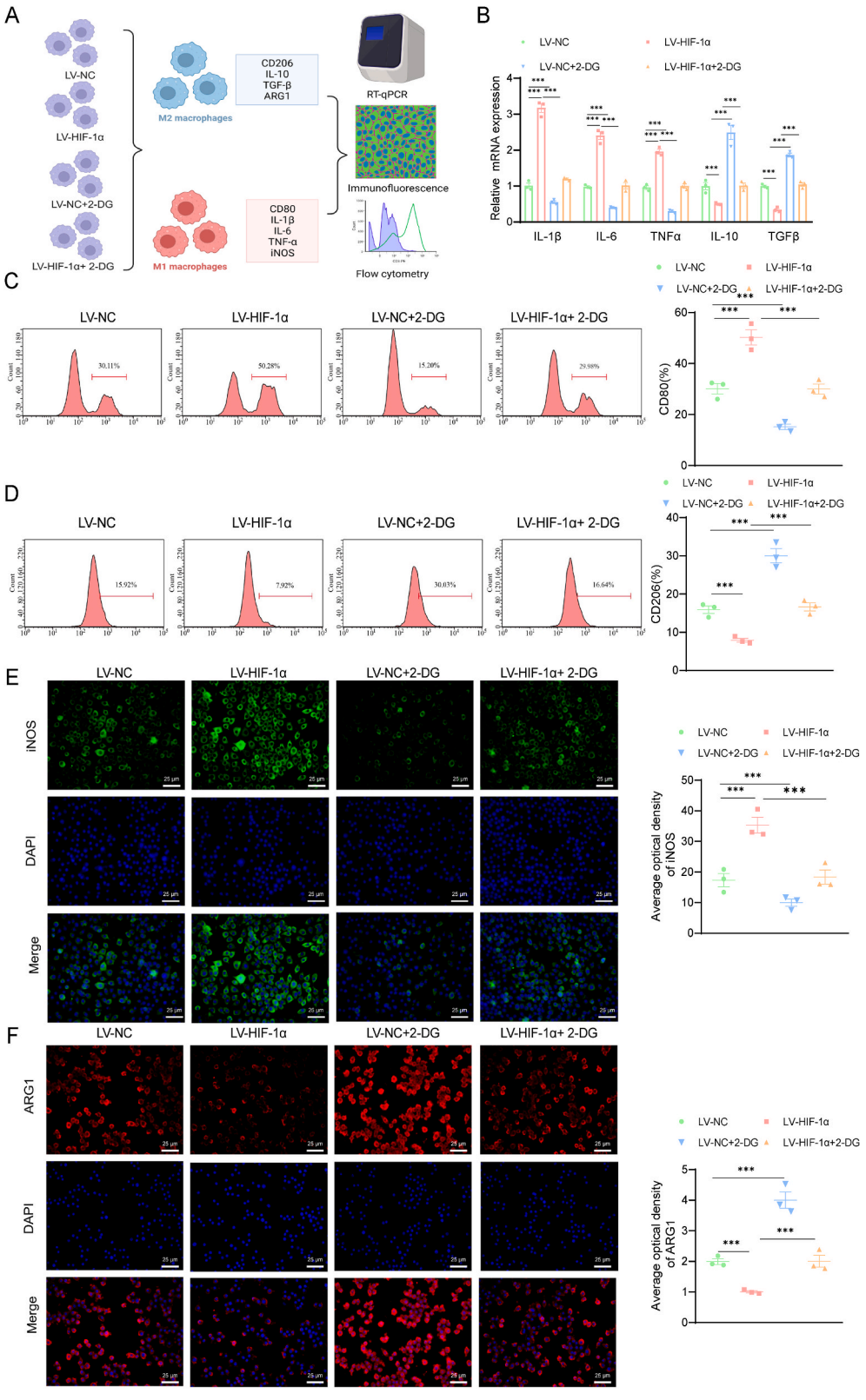

(caption on next page)

Fig. 4. Influence of HIF-1α/glycolysis pathway on Mψ polarization. Note: (A) Molecular mechanism of Mψ polarization influenced by HIF-1α/glycolysis pathway; (B) mRNA levels of IL-1β, IL-6, TNFα, IL-10, and TGFβ in RAW264.7 cells from different groups measured by RT-qPCR; (C) Proportion of CD80-positive RAW264.7 cells from different groups measured by flow cytometry; (D) Proportion of CD206-positive RAW264.7 cells from different groups measured by flow cytometry; (E) Protein expression of iNOS in RAW264.7 cells from different groups detected by immunofluorescence, scale bar: 25 μm; (F) Protein expression of ARG1 in RAW264.7 cells from different groups detected by immunofluorescence, scale bar: 25 μm. The cell experiments were performed in triplicate, and the values are presented as mean ± standard deviation. ***$P < 0.001$.

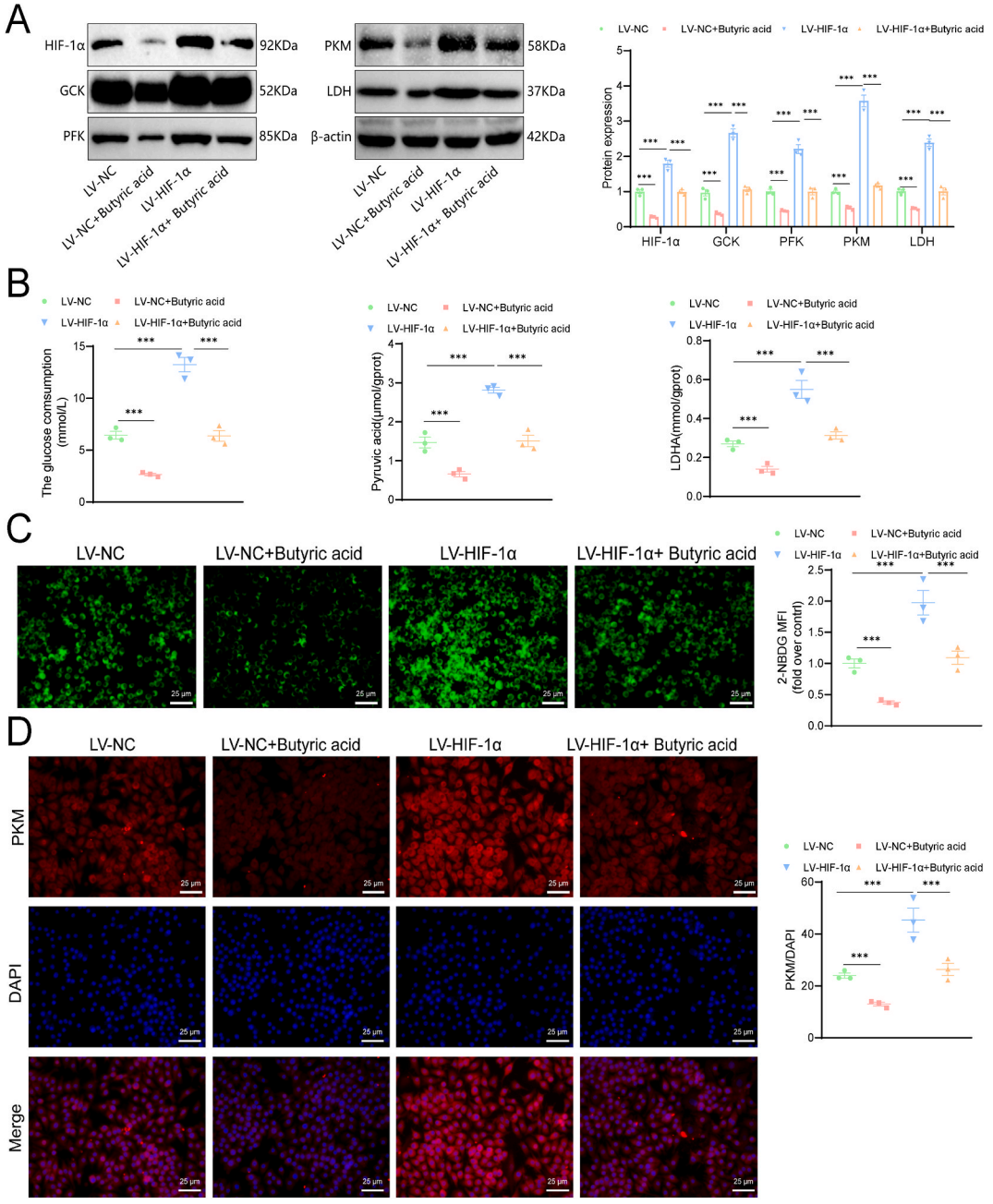

Fig. 5. Impact of HIF-1α overexpression on the glycolytic pathway. Note: (A) Protein expression of HIF-1α, GCK, PFK, PKM, and LDH in RAW264.7 cells of each group as detected by Western blot; (B) Glucose consumption, levels of pyruvate and LDHA in RAW264.7 cells of each group measured through ELISA; (C) Glucose uptake by RAW264.7 cells of each group visualized using immunofluorescence, scale bar: 25 μm; (D) Protein expression of PKM in RAW264.7 cells of each group detected through immunofluorescence, scale bar: 25 μm. Cell experiments were repeated 3 times, and values are presented as mean ± standard deviation. ***$P < 0.001$.

butyric acid, compared to the LV-NC control group. Conversely, the LV-HIF-1α group showed significant upregulation of these proteins. Furthermore, compared to the LV-HIF-1α group, cells treated with LV-HIF-1α+butyric acid exhibited a significant reduction in HIF-1α, GCK, PFK, PKM, and LDH protein expression (Fig. 5A). ELISA results demonstrated that glucose consumption, acetate, and LDHA levels were significantly reduced in cells treated with LV-NC + butyric acid compared to the LV-NC control group. Conversely, the LV-HIF-1α group showed significant increases in these parameters. Moreover, glucose consumption, acetate, and LDHA levels were significantly decreased in cells treated with LV-HIF-1α+butyric acid compared to the LV-HIF-1α group (Fig. 5B). Immunofluorescence analysis of glucose uptake revealed that LV-NC + butyric acid cells displayed a significant reduction in 2-NBDG uptake compared to the LV-NC control group. Conversely, the LV-HIF-1α group showed a significant increase in 2-NBDG uptake. Furthermore, cells treated with LV-HIF-1α+butyric acid exhibited a significant reduction in 2-NBDG uptake compared to the LV-HIF-1α group (Fig. 5C). Immunofluorescence analysis of PKM protein expression in cells showed that LV-NC + butyric acid cells had significantly lower PKM protein expression compared to the LV-NC control group. Conversely, the LV-HIF-1α group showed a significant increase in PKM expression. Moreover, cells treated with LV-HIF-1α+butyric acid exhibited a significant decrease in PKM protein expression compared to the LV-HIF-1α group (Fig. 5D).

In summary, under hypoxic conditions, butyric acid inhibits the HIF-1α/glycolytic pathway, thereby promoting M2 Mψ activation and regulating Mψ polarization.

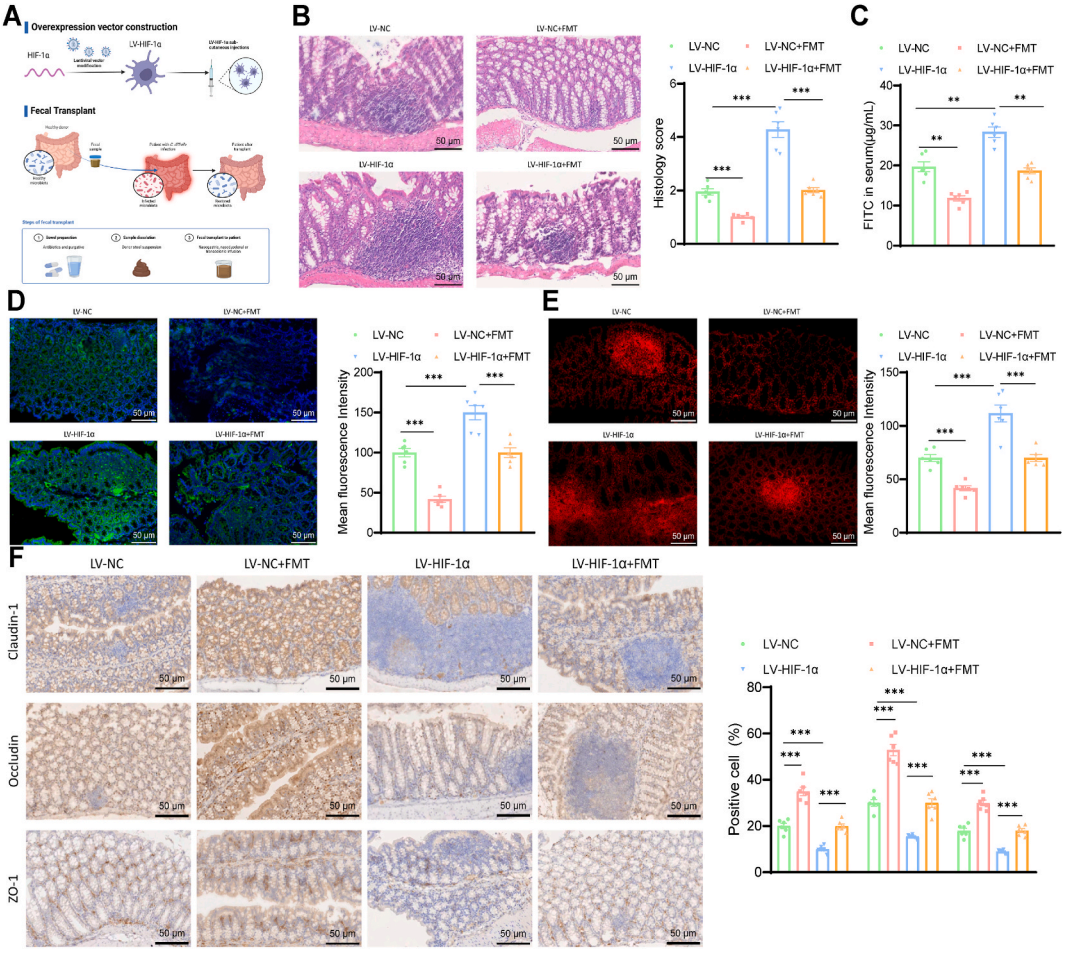

Fig. 6. The effects of firmicutes and HIF-1α overexpression on intrinsic mucosal barrier injury in mice induced by high-altitude hypoxia. Note: (A) Technical flowchart for establishing a mouse model of intestinal mucosal barrier injury induced by high-altitude hypoxia; (B) H&E staining to evaluate the morphology and structure of colonic cells in each group, scale bar = 50 μm; (C) FITC-D4 permeability in colon tissue of each group; (D) Pimonidazole staining to detect the expression of hypoxia probe signal intensity in colon tissue of each group, scale bar = 50 μm; (E) Fluorescent staining to measure the levels of ROS in colon tissue of each group, scale bar = 50 μm; (F) Immunohistochemical analysis of the protein expression of Claudin-1, Occludin, and ZO-1 in colon tissue of each group, scale bar = 50 μm. Each group consisted of 6 mice, and the values are presented as mean ± standard deviation. ***$P < 0.001$.

3.6. Firmicutes mitigate intrinsic mucosal barrier injury in high-altitude hypoxia mice through inhibition of the HIF-1α/glycolysis pathway

Cellular experiments demonstrate that butyrate can inhibit HIF-1α/glycolytic pathway Mψ polarization. Butyrate is a crucial short-chain fatty acid (SCFA) produced by the gut microbiota, primarily by bacteria within the phylum Firmicutes [67–69]. The fermentation of dietary fibers by gut Firmicutes generates short-chain fatty acids (SCFAs) such as butyrate, propionate, and acetate, with butyrate being the predominant SCFA produced [70]. Butyrate of microbial origin is primarily synthesized by bacteria belonging to the Firmicutes classes Clostridium _ IV and Clostridium _ XIVa, including Faecalibacterium prausnitzii and Eubacterium rectale, which are essential members of the human gut microbiota, representing 5–15 % of bacteria detected in healthy fecal samples and serving as significant producers of butyrate. Additionally, the Firmicutes genera Eubacterium, Faecalibacterium, and Roseburia are reported to be butyrate-producing Firmicutes species [71,72]. These bacteria play pivotal roles in maintaining gut health, modulating local and systemic immune responses, and safeguarding intestinal barrier integrity [67–69]. Butyric acid serves as the primary energy source for colon cells and possesses anti-inflammatory and anti-cancer properties, potentially influencing the gut-brain axis [64]. Hence, we conducted intestinal flora transplantation of firmicutes.

Using the previous modeling method, we established a mouse model of high-altitude hypoxia-induced intestinal mucosal barrier injury. By employing intestinal flora transplantation, we investigated how firmicutes, through the HIF-1α/glycolysis pathway, mediate Mψ polarization and alleviate intrinsic mucosal barrier injury in high-altitude hypoxia mice. Fig. 6A illustrates the construction of LV-HIF-1α and intestinal flora transplantation. H&E staining results demonstrated that the LV-NC group and LV-HIF-1α+FMT group exhibited increased crypt spacing, gland hyperplasia, disordered intestinal gland arrangement, and mucosal infiltration of inflammation. The LV-HIF-1α group displayed even greater crypt spacing, gland hyperplasia, pronounced disarray in intestinal gland arrangement, and severe mucosal infiltration of inflammation. In the LV-NC + FMT group, reduced crypt spacing and decreased mucosal infiltration of inflammation were observed (Fig. 6B). FITC-D4 permeability results showed a significant reduction in FITC-D4 leakage in the colon tissue of the LV-NC + FMT group compared to the LV-NC group, while FITC-D4 leakage significantly increased in the colon tissue of the LV-HIF-1α group. Furthermore, the colon tissue of the LV-HIF-1α+FMT group exhibited a significant increase in FITC-D4 leakage compared to the LV-HIF-1α group (Fig. 6C). The results of metronidazole staining revealed that the green fluorescence

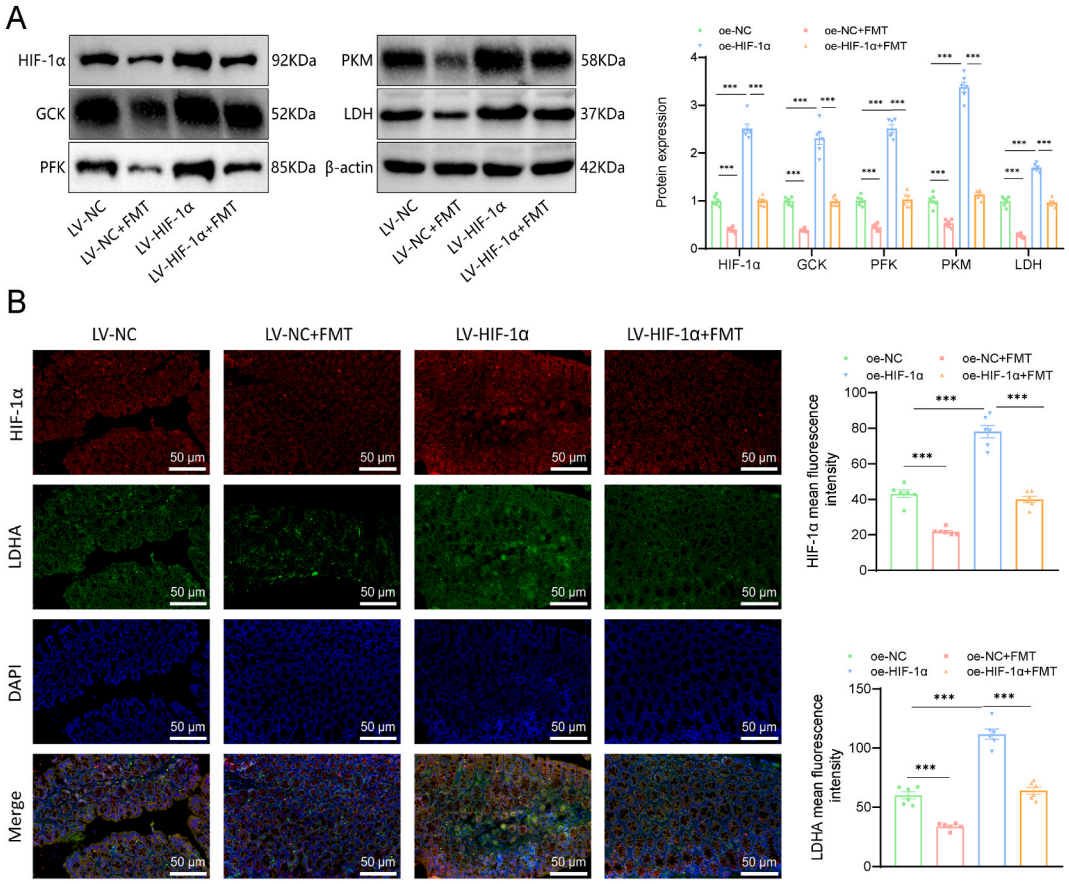

Fig. 7. Influence of firmicutes on HIF-1α/glycolytic pathway. Note: (A) Protein expression of HIF-1α, GCK, PFK, PKM, and LDHA in colon tissues of each group detected by Western blot; (B) Protein expression of HIF-1α and LDHA in colon tissues of each group visualized through immunofluorescence, scale bar: 50 μm. Each group consisted of 6 mice, and values are presented as mean ± standard deviation. ***$P < 0.001$.

in the colon tissue of the LV-NC + FMT group was significantly reduced compared to the LV-NC group, whereas the green fluorescence in the colon tissue of the LV-HIF-1α group was significantly increased. Additionally, the colon tissue of the LV-HIF-1α+FMT group displayed a marked increase in green fluorescence compared to the LV-HIF-1α group (Fig. 6D). Measurements of ROS revealed a significant decrease in red fluorescence in the colon tissue of the LV-NC + FMT group compared to the LV-NC group, whereas the colon tissue of the LV-HIF-1α group exhibited a notable increase in red fluorescence. Moreover, the colon tissue of the LV-HIF-1α+FMT group showed a significant increase in red fluorescence compared to the LV-HIF-1α group (Fig. 6E). Immunohistochemistry results indicated that protein expression of Claudin-1, Occludin, and ZO-1 in the colon tissue of the LV-NC + FMT group was significantly upregulated compared to the LV-NC group, while protein expression of Claudin-1, Occludin, and ZO-1 in the colon tissue of the LV-HIF-1α group was significantly downregulated. Furthermore, the colon tissue of the LV-HIF-1α+FMT group exhibited a significant upregulation in protein expression of Claudin-1, Occludin, and ZO-1 when compared to the LV-HIF-1α group (Fig. 6F).

Overall, our results demonstrate the successful establishment of a mouse model of high-altitude hypoxia-induced intrinsic mucosal barrier injury. Meanwhile, firmicutes can alleviate the intrinsic mucosal barrier injury caused by high-altitude hypoxia, whereas overexpression of HIF-1α may aggravate the injury.

Next, we investigated the impact of firmicutes on the HIF-1α/glycolysis pathway. Western blot experiments revealed a significant decrease in protein expression of HIF-1α, GCK, PFK, PKM, and LDH in the colon tissue of the LV-NC + FMT group compared to the LV-NC group. Conversely, the colon tissue of the LV-HIF-1α group showed a significant increase in protein expression of HIF-1α, GCK, PFK, PKM, and LDH. Additionally, the colon tissue of the LV-HIF-1α+FMT group exhibited a significant upregulation in protein expression of HIF-1α, GCK, PFK, PKM, and LDH when compared to the LV-HIF-1α group (Fig. 7A). Immunofluorescence detection of HIF-1α and LDHA protein expression in colon tissue showed a significant decrease in protein expression in the colon tissue of the LV-NC + FMT group compared to the LV-NC group. Moreover, protein expression of HIF-1α and LDHA in the colon tissue of the LV-HIF-1α group was significantly increased. Furthermore, the colon tissue of the LV-HIF-1α+FMT group exhibited a significant upregulation in protein expression of HIF-1α and LDHA compared to the LV-HIF-1α group (Fig. 7B).

In conclusion, firmicutes inhibit the HIF-1α/glycolysis pathway.

Finally, we investigated the influence of firmicutes on Mψ polarization through the HIF-1α/glycolysis pathway in mice with intrinsic mucosal barrier injury induced by high-altitude hypoxia. The results of flow cytometry revealed a significant decrease in the proportion of M1 Mψ cell marker CD80 in colon tissue of the LV-NC + FMT group compared to the LV-NC group. Conversely, the LV-HIF-1α group showed a significant increase in the proportion of CD80, and compared to the LV-HIF-1α group, the LV-HIF-1α+FMT group exhibited a significant increase in CD80 proportion (Fig. 8A). Additionally, compared to the LV-NC group, the LV-NC + FMT group showed a significant increase in the proportion of CD206, a cell marker for M2 Mψ, in colon tissue. However, the LV-HIF-1α group exhibited a significant decrease in CD206 proportion, and compared to the LV-HIF-1α group, the LV-HIF-1α+FMT group demonstrated a significant decrease in CD206 proportion (Fig. 8B). The immunofluorescence results displayed significant downregulation of iNOS protein expression in colon tissue of the LV-NC + FMT group compared to the LV-NC group. Conversely, the LV-HIF-1α group showed a significant upregulation of iNOS protein expression, and compared to the LV-HIF-1α group, the LV-HIF-1α+FMT group exhibited a significant upregulation of iNOS protein expression (Fig. 8C and D). Moreover, compared to the LV-NC group, the LV-NC + FMT group displayed a significant upregulation of ARG1 protein expression in colon tissue, while the LV-HIF-1α group demonstrated a significant downregulation of ARG1 protein expression. Likewise, compared to the LV-HIF-1α group, the LV-HIF-1α+FMT group exhibited a significant downregulation of ARG1 protein expression (Fig. 8E and F). The results of RT-qPCR and ELISA showed that in colon tissue of the LV-NC + FMT group, the mRNA levels and content of M1 Mψ cytokines IL-1β, IL-6, and TNFα were significantly reduced, while the mRNA levels and content of M2 Mψ cytokines IL-10 and TGFβ were significantly increased. On the other hand, the LV-HIF-1α group exhibited a significant upregulation of IL-1β, IL-6, and TNFα mRNA levels and content, along with a significant decrease in IL-10 and TGFβ mRNA levels and content. Furthermore, compared to the LV-HIF-1α group, the LV-HIF-1α+FMT group showed a significant upregulation of IL-1β, IL-6, and TNFα mRNA levels and content, as well as a significant decrease in IL-10 and TGFβ mRNA levels and content (Fig. 8G and H). These results indicate that firmicutes can inhibit the activation of M1 Mψ and promote the activation of M2 Mψ, thereby alleviating the intrinsic mucosal barrier injury in mice under high-altitude hypoxia.

4. Discussion

This study aims to investigate the molecular mechanisms of intrinsic mucosal barrier injury induced by high-altitude hypoxia (Fig. 9). We explored the involvement of Mψ in this process by studying the regulatory role of HIF-1α-mediated glycolysis reprogramming in firmicutes. Using a high-altitude hypoxia mouse model and extensive experimental data, we identified key cell types, proteins, and metabolic pathways involved in intrinsic mucosal barrier injury. This study provides significant insights into the molecular mechanisms of high-altitude hypoxia.

Prior research has confirmed the crucial role of Mψ in intrinsic mucosal barrier injury [73–75]. Our single-cell transcriptome sequencing analysis also revealed the importance of Mψ as a key cell type in this injury. The polarization pattern of Mψ plays a critical role in high-altitude hypoxia-induced intrinsic mucosal barrier injury, possibly through the modulation of HIF-1α and glycolysis pathways [76–78]. Previous studies have shown that in cultures of hypoxia-tolerant animal non-activated Mψ, the expression of VEGF and CD11b is higher, while the expression of Tnfa, Il1b, and Epas1 is lower. Moreover, the levels of HIF-1α mRNA and protein expression are comparable. In contrast, in lipopolysaccharide (LPS)-activated Mψ cultures of hypoxia-susceptible animals, the expression levels of Hif1a and CCR7 are higher compared to the hypoxia-tolerant group. Additionally, activation is associated with an increase in the content of HIF-1α in the cell culture medium. This disparity suggests a tendency for hypoxia-susceptible animals to promote inflammatory Mψ polarization [13].

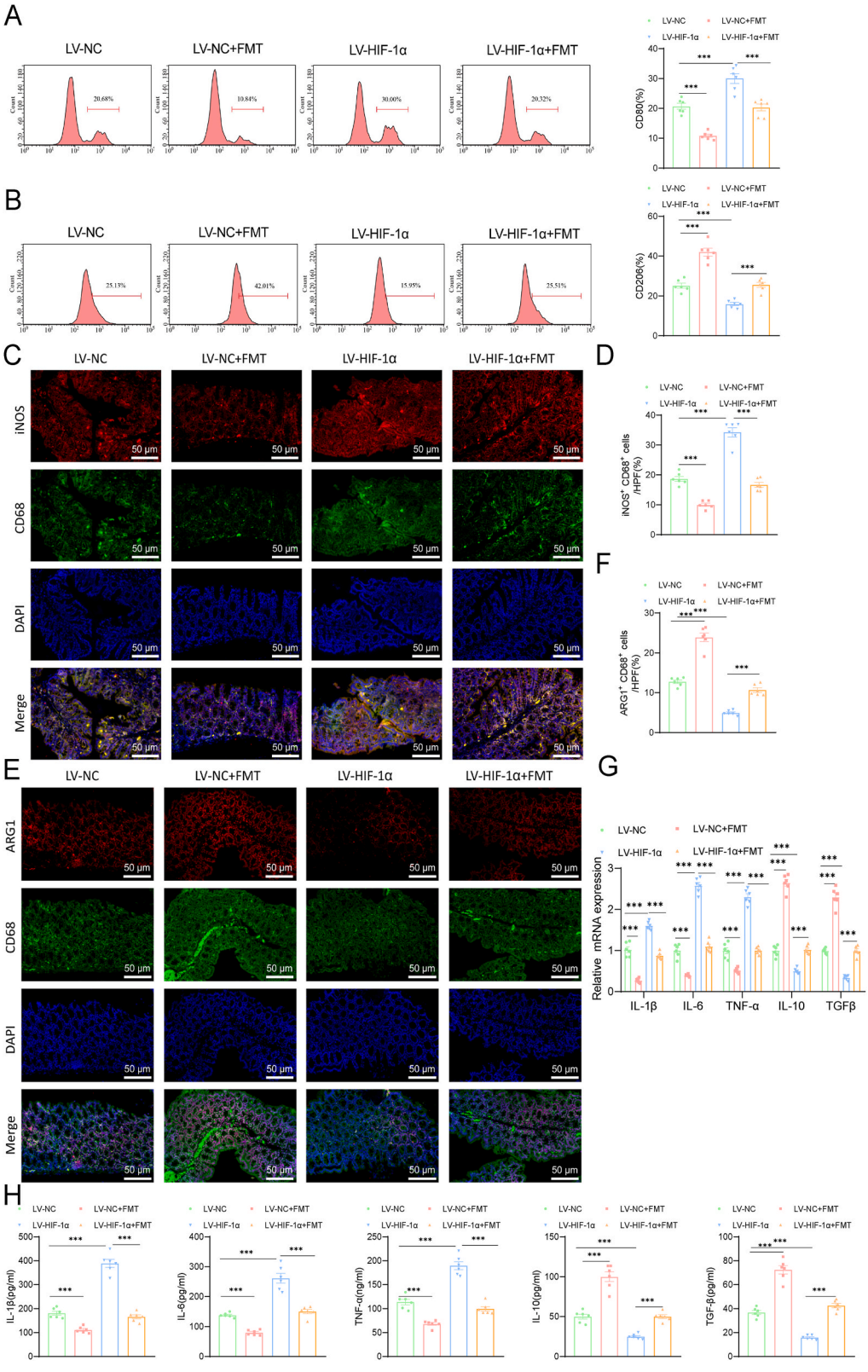

(caption on next page)

Fig. 8. Influence of firmicutes on Mψ polarization through HIF-1α/glycolysis. Note: (A) Proportion of CD80 in colon tissues of mice from each group analyzed by flow cytometry; (B) Proportion of CD206 in colon tissues of mice from each group analyzed by flow cytometry; (C–D) Protein expression of iNOS in colon tissues of mice from each group determined through immunofluorescence, scale bar: 50 μm; (E–F) Protein expression of ARG1 in colon tissues of mice from each group determined through immunofluorescence, scale bar: 50 μm; (G) mRNA levels of IL-1β, IL-6, TNFα, IL-10, and TGFβ in colon tissues of mice from each group analyzed by RT-qPCR; (H) Levels of IL-1β, IL-6, TNFα, IL-10, and TGFβ in serum of mice from each group measured by ELISA. Each group consisted of 6 mice, and values are presented as mean ± standard deviation. ***$P < 0.001$.

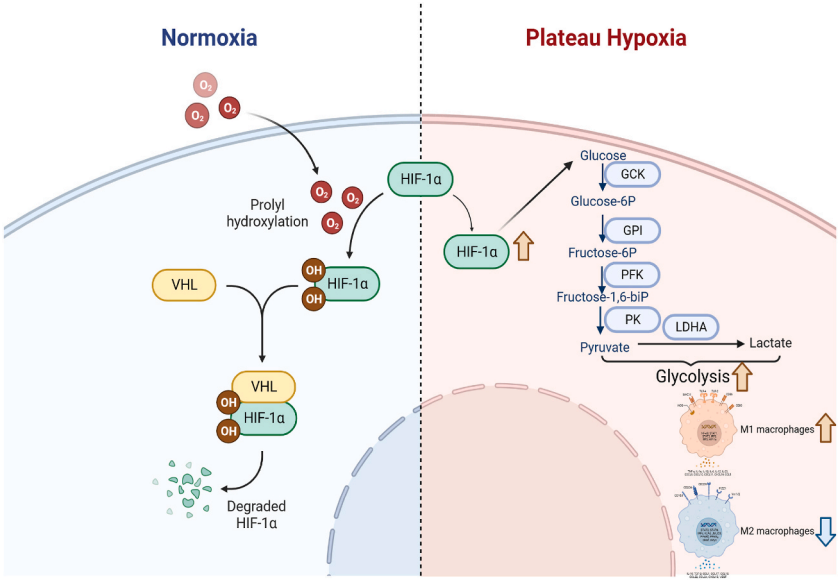

Fig. 9. Molecular mechanism of firmicutes involvement in Mψ polarization through HIF-1α/glycolysis pathway in high-altitude hypoxia-induced intrinsic mucosal barrier injury.

Interestingly, research indicates that hypoxia can induce or exacerbate inflammation, and the activation of HIF-1α can exacerbate intestinal inflammation. For example, frequent high-altitude activities are associated with gastrointestinal inflammation [79]. Hypoxia markers such as HIF-1α, Mψ Inflammatory Protein-3α (MIP-3α), and Vascular Endothelial Growth Factor (VEGF) are significantly elevated in colonic epithelial tissues and serum of pediatric and adult patients with active inflammatory bowel disease, positively correlating with histological severity [80]. HIF-1α has been shown to play a crucial regulatory role in intrinsic mucosal barrier injury [81,82]. This study extensively explores the molecular mechanisms of intrinsic mucosal barrier injury in the high-altitude hypoxia environment, with a particular focus on the impact of firmicutes on Mψ polarization through the regulation of HIF-1α and glycolysis pathways. This research provides a new perspective on how the gut microbiota affects host physiology in extreme environments. Compared to previous studies focused on the general interaction between the gut microbiota and the intestinal mucosal barrier, our study provides a deeper insight at the molecular level. By combining single-cell transcriptome sequencing with proteomics and metabolomics analysis, this multidimensional approach allows us to accurately identify Mψ as a key cell type in high-altitude hypoxia-induced intrinsic mucosal barrier injury [83,84].

Previous research has demonstrated the critical role of the glycolysis pathway in regulating the integrity of the intestinal mucosal barrier [85,86]. This study confirms that glycolysis is a key metabolic pathway in high-altitude hypoxia-induced intrinsic mucosal barrier injury and reveals its interaction with HIF-1α [87–89]. This finding deepens our understanding of the mechanisms of intrinsic mucosal barrier injury from a metabolic perspective [90].

This study has the following innovations: firstly, we clearly identified Mψ as a key cell type in high-altitude hypoxia-induced intrinsic mucosal barrier injury through single-cell transcriptome sequencing analysis. Secondly, we revealed that firmicutes regulate Mψ polarization through the HIF-1α/glycolysis pathway, thus alleviating intrinsic mucosal barrier injury. Finally, we extensively investigated the key roles of HIF-1α and the glycolysis pathway in intrinsic mucosal barrier injury.

The scientific value of this study lies in revealing how firmicutes mediate Mψ polarization through the regulation of glycolysis, thus alleviating high-altitude hypoxia-induced intrinsic mucosal barrier injury. These findings are crucial for understanding the role of the gut microbiota in intrinsic mucosal barrier injury and provide important clues for further research on the pathogenesis of inflammation-related diseases involving the gut microbiota.

From a clinical perspective, low temperature and low pressure hypoxia are characteristic of high-altitude environments, posing significant health challenges to over 1.4 billion people globally. Upper gastrointestinal bleeding caused by peptic ulcer disease appears to be a common issue in high-altitude regions. Numerous studies indicate that exposure to high altitudes can increase gastrointestinal inflammation, oxidative stress, and gut permeability, leading to alterations in gut microbiota composition and activity. Therefore,

exploring the molecular mechanisms underlying intestinal mucosal barrier damage induced by high-altitude hypoxia is beneficial for understanding the pathogenesis of diseases. The findings of this study hold promise for offering new insights into the prevention and treatment of intestinal mucosal barrier damage resulting from high-altitude hypoxia. Our research suggests that modulation of Mψ polarization and glycolytic metabolism may help restore impaired intestinal mucosal barrier function, consequently reducing the severity of inflammation and tissue damage caused by high-altitude hypoxia. This study delves into the relationship between Mψ metabolic reprogramming and intestinal mucosal barrier damage induced by high-altitude hypoxia, providing new molecular insights into the pathogenic process of high-altitude hypoxia, which is crucial for the health management of high-altitude residents and patients with high-altitude sickness. Additionally, the outcomes of this research are poised to further the development of treatment strategies in clinical research, offering a scientific basis for improving the health status of high-altitude residents and aiding in the prevention of altitude-related gastrointestinal diseases. Therefore, targeted therapies focusing on Firmicutes bacteria and butyric acid may represent novel treatment options for gastrointestinal diseases in high-altitude regions, facilitating the development of targeted therapies involving relevant microorganisms and metabolites.

However, this study has limitations. For example, using a mouse model to study high-altitude hypoxia-induced intrinsic mucosal barrier injury limits direct verification of the relevant mechanisms in humans. In addition, this study only focused on the role of Mψ in intrinsic mucosal barrier injury, while the involvement and regulatory mechanisms of other immune cell types need further investigation.

Looking ahead, future research can further investigate the interaction between the gut microbiota and Mψ, as well as the roles of other immune cell types in intrinsic mucosal barrier injury. Furthermore, studying the regulatory mechanisms of firmicutes and other microbial species on the intestinal mucosal barrier function will contribute to the development of new therapeutic approaches and drug targets for high-altitude hypoxia-related diseases.

Funding

This study was supported by Cultivation Fund of National Natural Science Foundation (Grant No. qiankehe2018-5764-11), Doctor Foundation of Guizhou Provincial People's Hospital (No.GZSYBS(2017)09).

Data availability

All data can be provided as needed.

Ethical statement

All animal experiments were approved by our institution's Animal Ethics Committee and complied with local guidelines for the welfare and use of laboratory animals (No. 2020-413).

Consent to participate

Not applicable.

Consent for publication

Not applicable.

CRediT authorship contribution statement

Fang Yan: Writing – review & editing. **Wen-qiang Yuan:** Writing – review & editing. **Shi-min Wu:** Writing – review & editing. **Yun-han Yang:** Writing – review & editing. **De-jun Cui:** Writing – review & editing.

Declaration of competing interest

The authors declare that they have no known competing financial interests or personal relationships that could have appeared to influence the work reported in this paper.

Acknowledgment

None.

Appendix A. Supplementary data

Supplementary data to this article can be found online at https://doi.org/10.1016/j.heliyon.2024.e38220.

References

[1] M.I.B. Debenham, J.N. Smuin, T.D.A. Grantham, P.N. Ainslie, B.H. Dalton, Hypoxia and standing balance, Eur. J. Appl. Physiol. 121 (4) (2021) 993–1008, https://doi.org/10.1007/s00421-020-04581-5.

[2] C.J. Doherty, J.C. Chang, B.P. Thompson, E.R. Swenson, G.E. Foster, P.B. Dominelli, The impact of acetazolamide and methazolamide on exercise performance in normoxia and hypoxia, High Alt. Med. Biol. 24 (1) (2023) 7–18, https://doi.org/10.1089/ham.2022.0134.

[3] Z.J. McKenna, F. Gorini Pereira, T.L. Gillum, F.T. Amorim, M.R. Deyhle, C.M. Mermier, High-altitude exposures and intestinal barrier dysfunction, Am. J. Physiol. Regul. Integr. Comp. Physiol. 322 (3) (2022) R192–R203, https://doi.org/10.1152/ajpregu.00270.2021.

[4] X. Li, J. Zhang, G. Liu, G. Wu, R. Wang, J. Zhang, High altitude hypoxia and oxidative stress: the new hope brought by free radical scavengers, Life Sci. 336 (2024) 122319, https://doi.org/10.1016/j.lfs.2023.122319.

[5] K.P. Mishra, J. Bakshi, Physiological benefits of Akkermansia muciniphila under high-altitude hypoxia, Appl. Microbiol. Biotechnol. 107 (1) (2023) 1–8, https://doi.org/10.1007/s00253-022-12305-2.

[6] J. Cheng, Y. Sun, J. He, Z. Wang, W. Li, R. Wang, The mechanism of colon tissue damage mediated by HIF-1α/NF-κB/STAT1 in high-altitude environment, Front. Physiol. 13 (2022) 933659, https://doi.org/10.3389/fphys.2022.933659. Published 2022 Sep. 9.

[7] J. Li, X. Jiang, H. Li, M. Gelinsky, Z. Gu, Tailoring materials for modulation of macrophage fate, Adv Mater 33 (12) (2021) e2004172, https://doi.org/10.1002/adma.202004172.

[8] Z. Yekhtin, I. Khuja, D. Meiri, R. Or, O. Almogi-Hazan, Differential effects of D9 tetrahydrocannabinol (THC)- and cannabidiol (CBD)-Based cannabinoid treatments on macrophage immune function in vitro and on gastrointestinal inflammation in a murine model, Biomedicines 10 (8) (2022) 1793, https://doi.org/10.3390/biomedicines10081793. Published 2022 Jul 26.

[9] M. Li, J. Yu, G. Guo, H. Shen, Interactions between macrophages and biofilm during Staphylococcus aureus-associated implant infection: difficulties and solutions, J. Innate Immun. 15 (1) (2023) 499–515, https://doi.org/10.1159/000530385.

[10] K.A. Sharkey, G.M. Mawe, The enteric nervous system, Physiol. Rev. 103 (2) (2023) 1487–1564, https://doi.org/10.1152/physrev.00018.2022.

[11] A. Ignacio, K. Shah, J. Bernier-Latmani, et al., Small intestinal resident eosinophils maintain gut homeostasis following microbial colonization, Immunity 55 (7) (2022) 1250–1267.e12, https://doi.org/10.1016/j.immuni.2022.05.014.

[12] J.F. Staab, J.M. Lemme-Dumit, R. Latanich, M.F. Pasetti, N.C. Zachos, Co-Culturing human intestinal enteroid monolayers with innate immune cells, Methods Mol. Biol. 2650 (2023) 207–223, https://doi.org/10.1007/978-1-0716-3076-1_16.

[13] D. Dzhalilova, A. Kosyreva, A. Lokhonina, et al., Molecular and phenotypic distinctions of macrophages in tolerant and susceptible to hypoxia rats, PeerJ 11 (2023) e16052, https://doi.org/10.7717/peerj.16052. Published 2023 Oct 10.

[14] S. El Alam, E. Pena, D. Aguilera, P. Siques, J. Brito, Inflammation in pulmonary hypertension and edema induced by hypobaric hypoxia exposure, Int. J. Mol. Sci. 23 (20) (2022) 12656, https://doi.org/10.3390/ijms232012656. Published 2022 Oct 21.

[15] J.P. Richalet, F. Jeny, P. Callard, J.F. Bernaudin, High-altitude pulmonary edema: the intercellular network hypothesis, Am. J. Physiol. Lung Cell Mol. Physiol. 325 (2) (2023) L155–L173, https://doi.org/10.1152/ajplung.00292.2022.

[16] J. Bai, L. Li, Y. Li, L. Zhang, Genetic and immune changes in Tibetan high-altitude populations contribute to biological adaptation to hypoxia, Environ. Health Prev. Med. 27 (2022) 39, https://doi.org/10.1265/ehpm.22-00040.

[17] X. Huang, Z. Chen, Z. Luo, et al., PFKFB3 downregulation aggravates Angiotensin II-induced podocyte detachment, Ren. Fail. 45 (1) (2023) 2230318, https://doi.org/10.1080/0886022X.2023.2230318.

[18] T.Y. Huang, M. Hirota, D. Sasaki, et al., Phosphoenolpyruvate regulates the Th17 transcriptional program and inhibits autoimmunity, Cell Rep. 42 (3) (2023) 112205, https://doi.org/10.1016/j.celrep.2023.112205.

[19] M. Schilperoort, D. Ngai, M. Katerelos, D.A. Power, I. Tabas, PFKFB2-mediated glycolysis promotes lactate-driven continual efferocytosis by macrophages, Nat. Metab. 5 (3) (2023) 431–444, https://doi.org/10.1038/s42255-023-00736-8.

[20] J. Xu, C. Gao, Y. He, et al., NLRC3 expression in macrophage impairs glycolysis and host immune defense by modulating the NF-κB-NFAT5 complex during septic immunosuppression, Mol. Ther. 31 (1) (2023) 154–173, https://doi.org/10.1016/j.ymthe.2022.08.023.

[21] T. Gauthier, C. Yao, T. Dowdy, et al., TGF-β uncouples glycolysis and inflammation in macrophages and controls survival during sepsis, Sci. Signal. 16 (797) (2023) eade0385, https://doi.org/10.1126/scisignal.ade0385.

[22] K. Xu, N. Yin, M. Peng, et al., Glycolysis fuels phosphoinositide 3-kinase signaling to bolster T cell immunity, Science 371 (6527) (2021) 405–410, https://doi.org/10.1126/science.abb2683.

[23] K.L. Tomlinson, S.A. Riquelme, S.U. Baskota, et al., Staphylococcus aureus stimulates neutrophil itaconate production that suppresses the oxidative burst, Cell Rep. 42 (2) (2023) 112064, https://doi.org/10.1016/j.celrep.2023.112064.

[24] A. Andoh, A. Nishida, Alteration of the gut microbiome in inflammatory bowel disease, Digestion 104 (1) (2023) 16–23, https://doi.org/10.1159/000525925.

[25] D. Povero, Y. Chen, S.M. Johnson, et al., HILPDA promotes NASH-driven HCC development by restraining intracellular fatty acid flux in hypoxia, J. Hepatol. 79 (2) (2023) 378–393, https://doi.org/10.1016/j.jhep.2023.03.041.

[26] Y.Y. He, X.M. Xie, H.D. Zhang, et al., Identification of hypoxia induced metabolism associated genes in pulmonary hypertension [published correction appears in Front Pharmacol. 2021 Dec 15;12:810178. doi: 10.3389/fphar.2021.810178, Front. Pharmacol. 12 (2021) 753727, https://doi.org/10.3389/fphar.2021.753727. Published 2021 Nov 5.

[27] H. Zhang, Y.B. Luo, W. Wu, et al., The molecular feature of macrophages in tumor immune microenvironment of glioma patients, Comput. Struct. Biotechnol. J. 19 (2021) 4603–4618, https://doi.org/10.1016/j.csbj.2021.08.019. Published 2021 Aug 14.

[28] Y.J. Zhou, X.F. Lu, H. Chen, et al., Single-cell transcriptomics reveals early molecular and immune alterations underlying the serrated neoplasia pathway toward colorectal cancer, Cell Mol Gastroenterol Hepatol 15 (2) (2023) 393–424, https://doi.org/10.1016/j.jcmgh.2022.10.001.

[29] S. Yu, M. Chen, L. Xu, E. Mao, S. Sun, A senescence-based prognostic gene signature for colorectal cancer and identification of the role of SPP1-positive macrophages in tumor senescence, Front. Immunol. 14 (2023) 1175490, https://doi.org/10.3389/fimmu.2023.1175490. Published 2023 Apr 6.

[30] J. Jiang, J. Xiang, M. Chen, et al., Distinct mechanisms of dysfunctional antigen-presenting DCs and monocytes by single-cell sequencing in multiple myeloma, Cancer Sci. 114 (7) (2023) 2750–2760, https://doi.org/10.1111/cas.15800.

[31] X. Li, Y. Zhi, J. Li, et al., Single-cell RNA sequencing to reveal non-parenchymal cell heterogeneity and immune network of acetaminophen-induced liver injury in mice, Arch. Toxicol. 97 (7) (2023) 1979–1995, https://doi.org/10.1007/s00204-023-03513-4.

[32] Z. Wan, X. Zhang, X. Jia, et al., Lactobacillus johnsonii YH1136 plays a protective role against endogenous pathogenic bacteria induced intestinal dysfunction by reconstructing gut microbiota in mice exposed at high altitude, Front. Immunol. 13 (2022) 1007737, https://doi.org/10.3389/fimmu.2022.1007737. Published 2022 Oct 10.

[33] X. Li, W. Chen, J. Feng, B. Zhao, The effects of HIF-1α overexpression on renal injury, immune disorders and mitochondrial apoptotic pathways in renal ischemia/reperfusion rats, Transl. Androl. Urol. 9 (5) (2020) 2157–2165, https://doi.org/10.21037/tau-20-918.

[34] X. Lou, J. Xue, R. Shao, et al., Fecal microbiota transplantation and short-chain fatty acids reduce sepsis mortality by remodeling antibiotic-induced gut microbiota disturbances, Front. Immunol. 13 (2023) 1063543, https://doi.org/10.3389/fimmu.2022.1063543. Published 2023 Jan 11.

[35] Z. Chen, S. He, Y. Wei, et al., Fecal and serum metabolomic signatures and gut microbiota characteristics of allergic rhinitis mice model, Front. Cell. Infect. Microbiol. 13 (2023) 1150043, https://doi.org/10.3389/fcimb.2023.1150043. Published 2023 Apr 25.

[36] Q. Zhu, Y. Han, X. Wang, et al., Hypoxia exacerbates intestinal injury and inflammatory response mediated by myeloperoxidase during Salmonella Typhimurium infection in mice, Gut Pathog. 15 (1) (2023) 62, https://doi.org/10.1186/s13099-023-00586-5. Published 2023 Nov 30.

[37] N. Liang, Y. Li, H.Y. Chung, Two natural eudesmane-type sesquiterpenes from Laggera alata inhibit angiogenesis and suppress breast cancer cell migration through VEGF- and Angiopoietin 2-mediated signaling pathways, Int. J. Oncol. 51 (1) (2017) 213–222, https://doi.org/10.3892/ijo.2017.4004.

[38] J. Wen, S. Wu, X. Ma, Y. Zhao, Zuojin Pill attenuates Helicobacter pylori-induced chronic atrophic gastritis in rats and improves gastric epithelial cells function in GES-1 cells, J. Ethnopharmacol. 285 (2022) 114855, https://doi.org/10.1016/j.jep.2021.114855.

[39] G.A. Walaas, S. Gopalakrishnan, I. Bakke, et al., Physiological hypoxia improves growth and functional differentiation of human intestinal epithelial organoids, Front. Immunol. 14 (2023) 1095812, https://doi.org/10.3389/fimmu.2023.1095812. Published 2023 Jan 27.
[40] Y. Hao, S. Hao, E. Andersen-Nissen, et al., Integrated analysis of multimodal single-cell data, Cell 184 (13) (2021) 3573–3587.e29, https://doi.org/10.1016/j.cell.2021.04.048.
[41] L. Ma, M.O. Hernandez, Y. Zhao, et al., Tumor cell biodiversity drives microenvironmental reprogramming in liver cancer, Cancer Cell 36 (4) (2019) 418–430.e6, https://doi.org/10.1016/j.ccell.2019.08.007.
[42] M.E. Ritchie, B. Phipson, D. Wu, et al., Limma powers differential expression analyses for RNA-sequencing and microarray studies, Nucleic Acids Res. 43 (7) (2015) e47, https://doi.org/10.1093/nar/gkv007.
[43] X.S. Liu, L.M. Zhou, L.L. Yuan, et al., NPM1 is a prognostic biomarker involved in immune infiltration of lung adenocarcinoma and associated with m6A modification and glycolysis [published correction appears in Front Immunol. 2021 Aug 31;12:751004. doi: 10.3389/fimmu.2021.751004, Front. Immunol. 12 (2021) 724741, https://doi.org/10.3389/fimmu.2021.724741. Published 2021 Jul 16.
[44] M. Deng, J. Sun, L. Peng, et al., Scutellarin acts on the AR-NOX axis to remediate oxidative stress injury in a mouse model of cerebral ischemia/reperfusion injury, Phytomedicine 103 (2022) 154214, https://doi.org/10.1016/j.phymed.2022.154214.
[45] N.F. Chi, T.H. Chang, C.Y. Lee, et al., Untargeted metabolomics predicts the functional outcome of ischemic stroke, J. Formos. Med. Assoc. 120 (1 Pt 1) (2021) 234–241, https://doi.org/10.1016/j.jfma.2020.04.026.
[46] J.Y. Hou, G.Z. Cao, L.L. Tian, et al., Integrated transcriptomics and metabolomics analysis reveals that C3 and C5 are vital targets of DuZhi Wan in protecting against cerebral ischemic injury, Biomed. Pharmacother. 155 (2022) 113703, https://doi.org/10.1016/j.biopha.2022.113703.
[47] G. Huang, J. Su, M. Zhang, et al., RhoB regulates the function of macrophages in the hypoxia-induced inflammatory response, Cell. Mol. Immunol. 14 (3) (2017) 265–275, https://doi.org/10.1038/cmi.2015.78.
[48] Z. Zhang, J. Wang, Y. Chen, et al., Activin a promotes myofibroblast differentiation of endometrial mesenchymal stem cells via STAT3-dependent Smad/CTGF pathway, Cell Commun. Signal. 17 (1) (2019) 45, https://doi.org/10.1186/s12964-019-0361-3. Published 2019 May 17.
[49] Y. Wang, Z. Zhou, Y. Liu, Z. Wang, Y. Kang, Inhibition of Smad3 promotes the healing of rotator cuff injury in a rat model, J. Orthop. Res. 39 (1) (2021) 204–218, https://doi.org/10.1002/jor.24768.
[50] H. Ni, H. Qin, C. Sun, et al., MiR-375 reduces the stemness of gastric cancer cells through triggering ferroptosis, Stem Cell Res. Ther. 12 (1) (2021) 325, https://doi.org/10.1186/s13287-021-02394-7. Published 2021 Jun 5.
[51] L. Shi, H. Chen, Y.Y. Qin, T.Q. Gan, K.L. Wei, Clinical and biologic roles of PDGFRA in papillary thyroid cancer: a study based on immunohistochemical and in vitro analyses, Int. J. Clin. Exp. Pathol. 13 (5) (2020) 1094–1107. Published 2020 May 1.
[52] H. Miwa, M. Shikami, M. Goto, et al., Leukemia cells demonstrate a different metabolic perturbation provoked by 2-deoxyglucose, Oncol. Rep. 29 (5) (2013) 2053–2057, https://doi.org/10.3892/or.2013.2299.
[53] T. Xu, M. Dong, H. Li, R. Zhang, X. Li, Elevated mRNA expression levels of DLGAP5 are associated with poor prognosis in breast cancer, Oncol. Lett. 19 (6) (2020) 4053–4065, https://doi.org/10.3892/ol.2020.11533.
[54] P. Zhou, W. Yu, C. Zhang, et al., Tiao-bu-fei-shen formula promotes downregulation of the caveolin 1-p38 mapk signaling pathway in COPD - associated tracheobronchomalacia cell model, J. Ethnopharmacol. 293 (2022) 115256, https://doi.org/10.1016/j.jep.2022.115256.
[55] S. Zou, C. Wang, Z. Cui, et al., β-Elemene induces apoptosis of human rheumatoid arthritis fibroblast-like synoviocytes via reactive oxygen species-dependent activation of p38 mitogen-activated protein kinase, Pharmacol. Rep. 68 (1) (2016) 7–11, https://doi.org/10.1016/j.pharep.2015.06.004.
[56] L. Liste-Calleja, M. Lecina, J. Lopez-Repullo, J. Albiol, C. Solà, J.J. Cairó, Lactate and glucose concomitant consumption as a self-regulated pH detoxification mechanism in HEK293 cell cultures, Appl. Microbiol. Biotechnol. 99 (23) (2015) 9951–9960, https://doi.org/10.1007/s00253-015-6855-z.
[57] I. Elia, J.H. Rowe, S. Johnson, et al., Tumor cells dictate anti-tumor immune responses by altering pyruvate utilization and succinate signaling in $CD8^+$ T cells, Cell Metab 34 (8) (2022) 1137–1150.e6, https://doi.org/10.1016/j.cmet.2022.06.008.
[58] H. Zhuang, Q. Lv, C. Zhong, et al., Tiliroside ameliorates ulcerative colitis by restoring the M1/M2 macrophage balance via the HIF-1α/glycolysis pathway, Front. Immunol. 12 (2021) 649463, https://doi.org/10.3389/fimmu.2021.649463. Published 2021 Mar 31.
[59] B. Yue, C. Song, L. Yang, et al., METTL3-mediated N6-methyladenosine modification is critical for epithelial-mesenchymal transition and metastasis of gastric cancer, Mol. Cancer 18 (1) (2019) 142, https://doi.org/10.1186/s12943-019-1065-4. Published 2019 Oct 13.
[60] Z. Wang, X. Zhang, L. Zhu, et al., Inulin alleviates inflammation of alcoholic liver disease via SCFAs-inducing suppression of M1 and facilitation of M2 macrophages in mice, Int Immunopharmacol 78 (2020) 106062, https://doi.org/10.1016/j.intimp.2019.106062.
[61] T. Wang, H. Liu, G. Lian, S.Y. Zhang, X. Wang, C. Jiang, HIF1α-Induced glycolysis metabolism is essential to the activation of inflammatory macrophages, Mediators Inflamm 2017 (2017) 9029327, https://doi.org/10.1155/2017/9029327.
[62] H. Semba, N. Takeda, T. Isagawa, et al., HIF-1α-PDK1 axis-induced active glycolysis plays an essential role in macrophage migratory capacity, Nat. Commun. 7 (2016) 11635, https://doi.org/10.1038/ncomms11635. Published 2016 May 18.
[63] G.M. Tannahill, A.M. Curtis, J. Adamik, et al., Succinate is an inflammatory signal that induces IL-1β through HIF-1α, Nature 496 (7444) (2013) 238–242, https://doi.org/10.1038/nature11986.
[64] Y.X. Wei, K.Y. Zheng, Y.G. Wang, Gut microbiota-derived metabolites as key mucosal barrier modulators in obesity, World J. Gastroenterol. 27 (33) (2021) 5555–5565, https://doi.org/10.3748/wjg.v27.i33.5555.
[65] G. Sorrentino, A. Perino, E. Yildiz, et al., Bile acids signal via TGR5 to activate intestinal stem cells and epithelial regeneration, Gastroenterology 159 (3) (2020) 956–968.e8, https://doi.org/10.1053/j.gastro.2020.05.067.
[66] P. Rodríguez-Viso, A. Domene, D. Vélez, V. Devesa, M. Zúñiga, V. Monedero, Lactic acid bacteria strains reduce in vitro mercury toxicity on the intestinal mucosa, Food Chem. Toxicol. 173 (2023) 113631, https://doi.org/10.1016/j.fct.2023.113631.
[67] F. Magne, M. Gotteland, L. Gauthier, et al., The firmicutes/bacteroidetes ratio: a relevant marker of gut dysbiosis in obese patients? Nutrients 12 (5) (2020) 1474, https://doi.org/10.3390/nu12051474. Published 2020 May 19.
[68] M.K. Stoeva, J. Garcia-So, N. Justice, et al., Butyrate-producing human gut symbiont, Clostridium butyricum, and its role in health and disease, Gut Microb. 13 (1) (2021) 1–28, https://doi.org/10.1080/19490976.2021.1907272.
[69] P. Louis, H.J. Flint, Formation of propionate and butyrate by the human colonic microbiota, Environ. Microbiol. 19 (1) (2017) 29–41, https://doi.org/10.1111/1462-2920.13589.
[70] Y. Fan, O. Pedersen, Gut microbiota in human metabolic health and disease, Nat. Rev. Microbiol. 19 (1) (2021) 55–71, https://doi.org/10.1038/s41579-020-0433-9.
[71] H.M. Hamer, D. Jonkers, K. Venema, S. Vanhoutvin, F.J. Troost, R.J. Brummer, Review article: the role of butyrate on colonic function, Aliment. Pharmacol. Ther. 27 (2) (2008) 104–119, https://doi.org/10.1111/j.1365-2036.2007.03562.x.
[72] V. Singh, G. Lee, H. Son, et al., Butyrate producers, "The Sentinel of Gut": their intestinal significance with and beyond butyrate, and prospective use as microbial therapeutics, Front. Microbiol. 13 (2023) 1103836, https://doi.org/10.3389/fmicb.2022.1103836. Published 2023 Jan 12.
[73] C. Gao, Y. Zhou, Z. Chen, et al., Turmeric-derived nanovesicles as novel nanobiologics for targeted therapy of ulcerative colitis, Theranostics 12 (12) (2022) 5596–5614, https://doi.org/10.7150/thno.73650. Published 2022 Jul 18.
[74] Q. Hou, J. Huang, H. Ayansola, H. Masatoshi, B. Zhang, Intestinal stem cells and immune cell relationships: potential therapeutic targets for inflammatory bowel diseases, Front. Immunol. 11 (2021) 623691, https://doi.org/10.3389/fimmu.2020.623691. Published 2021 Jan 20.
[75] S. Sun, X. Xu, L. Liang, et al., Lactic acid-producing probiotic Saccharomyces cerevisiae attenuates ulcerative colitis via suppressing macrophage pyroptosis and modulating gut microbiota, Front. Immunol. 12 (2021) 777665, https://doi.org/10.3389/fimmu.2021.777665. Published 2021 Nov 24.
[76] S.Z. Wu, G. Al-Eryani, D.L. Roden, et al., A single-cell and spatially resolved atlas of human breast cancers, Nat. Genet. 53 (9) (2021) 1334–1347, https://doi.org/10.1038/s41588-021-00911-1.
[77] S. Cheng, Z. Li, R. Gao, et al., A pan-cancer single-cell transcriptional atlas of tumor infiltrating myeloid cells, Cell 184 (3) (2021) 792–809.e23, https://doi.org/10.1016/j.cell.2021.01.010.

[78] R. Li, J.R. Ferdinand, K.W. Loudon, et al., Mapping single-cell transcriptomes in the intra-tumoral and associated territories of kidney cancer, Cancer Cell 40 (12) (2022) 1583–1599.e10, https://doi.org/10.1016/j.ccell.2022.11.001.
[79] S.R. Vavricka, G. Rogler, S. Maetzler, et al., High altitude journeys and flights are associated with an increased risk of flares in inflammatory bowel disease patients, J Crohns Colitis 8 (3) (2014) 191–199, https://doi.org/10.1016/j.crohns.2013.07.011.
[80] E.F. deZoeten, K.D. Battista, S.B. Colson, et al., Markers of hypoxia correlate with histologic and endoscopic severity of colitis in inflammatory bowel disease, Hypoxia 8 (2020) 1–12, https://doi.org/10.2147/HP.S219049. Published 2020 Feb 10.
[81] R. Liu, S.M. Wang, S.J. Guo, M.M. Ma, Y.L. Fu, Histone deacetylase inhibitor attenuates intestinal mucosal injury in fatally scalded rats, Ann. Transl. Med. 10 (2) (2022) 54, https://doi.org/10.21037/atm-21-5766 [published correction appears in Ann Transl Med. 2023 Aug 30;11(10):379. doi: 10.21037/atm-2023-14.
[82] L. Gu, J. Jiang, Z. Liu, et al., Intestinal recruitment of CCR6-expressing Th17 cells by suppressing miR-681 alleviates endotoxemia-induced intestinal injury and reduces mortality, Inflamm. Res. 72 (4) (2023) 715–729, https://doi.org/10.1007/s00011-023-01697-0.
[83] L. Song, F. Jiang, Y. Tian, et al., Integrated transcriptome, proteome and single-cell sequencing uncover the prognostic and immunological features of colony-stimulating factor 3 receptor in pan-cancer, J. Gene Med. 25 (10) (2023) e3508, https://doi.org/10.1002/jgm.3508.
[84] X. Gao, S. Wang, Y.F. Wang, et al., Long read genome assemblies complemented by single cell RNA-sequencing reveal genetic and cellular mechanisms underlying the adaptive evolution of yak, Nat. Commun. 13 (1) (2022) 4887, https://doi.org/10.1038/s41467-022-32164-9. Published 2022 Sep. 6.
[85] Y. Xia, L. Zhang, D.K.W. Ocansey, Q. Tu, F. Mao, X. Sheng, Role of glycolysis in inflammatory bowel disease and its associated colorectal cancer, Front. Endocrinol. 14 (2023) 1242991, https://doi.org/10.3389/fendo.2023.1242991. Published 2023 Oct 10.
[86] N. Tian, L. Hu, Y. Lu, et al., TKT maintains intestinal ATP production and inhibits apoptosis-induced colitis, Cell Death Dis. 12 (10) (2021) 853, https://doi.org/10.1038/s41419-021-04142-4. Published 2021 Sep. 17.
[87] Y. Geng, Y. Hu, F. Zhang, Y. Tuo, R. Ge, Z. Bai, Mitochondria in hypoxic pulmonary hypertension, roles and the potential targets, Front. Physiol. 14 (2023) 1239643, https://doi.org/10.3389/fphys.2023.1239643. Published 2023 Aug 14.
[88] D. Wang, F. Liu, W. Yang, et al., Meldonium ameliorates hypoxia-induced lung injury and oxidative stress by regulating platelet-type phosphofructokinase-mediated glycolysis, Front. Pharmacol. 13 (2022) 863451, https://doi.org/10.3389/fphar.2022.863451. Published 2022 Apr 5.
[89] G. Liu, Y. Li, N. Liao, et al., Energy metabolic mechanisms for high altitude sickness: downregulation of glycolysis and upregulation of the lactic acid/amino acid-pyruvate-TCA pathways and fatty acid oxidation, Sci. Total Environ. 894 (2023) 164998, https://doi.org/10.1016/j.scitotenv.2023.164998.
[90] X. Zhang, H. Wang, C. Xie, et al., Shenqi compound ameliorates type-2 diabetes mellitus by modulating the gut microbiota and metabolites, J Chromatogr B Analyt Technol Biomed Life Sci 1194 (2022) 123189, https://doi.org/10.1016/j.jchromb.2022.123189.